Dynamic Leader based Collective Intelligence for Maximum Power Point Tracking of PV Systems Affected by Partial Shading Condition

Bo Yang [1], Tao Yu [2], Xiaoshun Zhang [3,*], Hongchun Shu [1], Yiyan Sang [4], Lin Jiang [4]

[1] Faculty of Electric Power Engineering, Kunming University of Science and Technology, 650500 Kunming, China;
[2] College of Electric Power, South China University of Technology, 510640 Guangzhou, China;
[3] College of Engineering, Shantou University, 515063 Shantou, China;
[4] Department of Electrical Engineering & Electronics, University of Liverpool, Liverpool, L69 3GJ, United Kingdom;
* Correspondence: Xiaoshun Zhang, e-mail: xszhang1990@sina.cn

Abstract: This study presents a novel maximum power point tracking (MPPT) algorithm via dynamic leader based collective intelligence (DLCI) of PV systems affected by partial shading condition (PSC). Different from the conventional meta-heuristic algorithms, DLCI is consisted of multiple sub-optimizers, which can achieve a much wider exploration by fully collaborating the optimization ability of various searching mechanisms instead of a single searching mechanism. In order to achieve a deeper exploitation, the sub-optimizer with the current best solution is chosen as the dynamic leader for an efficient searching guidance to other sub-optimizers. Although the multiple sub-optimizers of DLCI will result in a higher computational complexity, it can offer an enhanced searching ability and a more stable convergence compared to that of conventional meta-heuristic algorithms. Since it does not reply on the system model, DLCI can be easily applied to other optimization tasks. Four case studies, including start-up test, step change in solar irradiation with constant temperature, gradual change in both solar irradiation and temperature, and daily field data of solar irradiation and temperature in Hong Kong, are undertaken. They attempt to evaluate the effectiveness and advantages of DLCI in comparison to that of conventional incremental conductance (INC) and eight typical meta-heuristic algorithms, e.g., genetic algorithm (GA), particle swarm optimization (PSO), artificial bees colony (ABC), Cuckoo search algorithm (CSA), grey wolf optimizer (GWO), moth-flame optimization (MFO), whale optimization algorithm (WOA), and teaching-learning-based optimization (TLBO), respectively. Lastly, a dSpace based hardware-in-the-loop (HIL) test is carried out to validate the implementation feasibility of DLCI based MPPT technique. Both the case studies and HIL test demonstrate that the searching ability of DLCI can be significantly improved via an effective coordination between multiple sub-optimizers, which can make the PV system generate more energy (up to 36.64%) and smaller power fluctuation (up to 21.17%) than other methods with a single searching mechanism.

Keywords: PV systems; MPPT; partial shading condition; dynamic leader based collective intelligence; HIL test

Nomenclature

Variables		*Abbreviations*	
V_{pv}	PV output voltage	**MPPT**	maximum power point tracking
I_{pv}	PV output current	**PV**	Photovoltaic
I_g	cell's photocurrent	**PSC**	partial shading condition
I_D	diode's photocurrent	**INC**	incremental conductance
I_S	cell's reverse saturation current	**CI**	collective intelligence
I_{RS}	d-q components of the grid current	**DLCI**	dynamic leader based collective intelligence
T_c	cell's absolute working temperature, K	**GA**	genetic algorithm
T_{ref}	cell's reference temperature, K	**PSO**	particle swarm optimization
S	total solar irradiation, W/m^2	**ABC**	artificial bees colony
E_g	bang-gap energy of the semiconductor used in the cell	**CSA**	Cuckoo search algorithm
N_p	number of panels connected in parallel	**TLBO**	teaching-learning-based optimization
N_s	number of panels connected in series	**GMPP**	global maximum power point
V_{oc}	open-circuit voltage of a single PV cell	**LMPP**	local maximum power point
$V_{reverse}$	reverse voltage drop on the shadowed cell	**GWO**	grey wolf optimizer

$\overrightarrow{V_i}$	velocity vector of the *i*th particle	**RES**	renewable energy system
r_1, r_2	random numbers	**P&O**	perturb & observe
$\overrightarrow{P_i}$	the individual best position of the *i*th particle	**DMPPT**	distributed maximum power point trackers
$\vec{G}$	the global best position of the whole swarm	**ACO**	ant colony optimization
$f_o^{best}(k)$	the fitness function of the best solution obtained by the *o*th sub-optimizer at the *k*th iteration	**SA**	simulate annealing
$\vec{X}_o^{worst}(k)$	the worst solution obtained by the oth sub-optimizer at the *k*th iteration	**WOA**	whale optimization algorithm
$\vec{X}_L^{best}(k)$	the best solution obtained by the dynamic leader at the *k*th iteration	**RMO**	radial movement optimization
Z	the set of all integers	**CSO**	cat swarm optimization
V_{Bdiode}	voltage drop of one bypass diode	**HIL**	hardware-in-the-loop
$\vec{X}$	position vector of the searching individual	***DLCI parameters***	
PV system parameters		n	number of sub-optimizers
q	electron charge, 1.60217733×10^{-19} Cb	N	population size
A	p-n junction ideality factor, between 1 and 5	$k_{\max}$	maximum iteration number
k	Boltzman's constant, 1.380658×10^{-23} J/K	a	adaption factor
k_i	cell's short-circuit current temperature coefficient	b	shape constant
R_s	cell's series resistance	c_1, c_2	acceleration coefficients
R_p	cell's parallel resistance	ω	inertia weight

1. Introduction

Renewable energy system (RES) is growing rapidly around the globe in the past decade due to the ever-increasing demand of energy, particularly in the booming economies like China and India, with an ambitious trend of energy efficiency improvement and carbon emission reduction [1-5]. In general, deployed RES usually involves various energy conversion technologies, e.g., hydro, wind, solar, biomass, tidal, wave, geothermal, etc. [6-8], which can provide a promising and effective solution for the emerging energy crisis of both developing and developed countries [9,10]. Among different RES, photovoltaic (PV) system has become a major and popular application thanks to its prominent merits of abundance of solar energy, pollution free, noiseless operation and low tear-and-wear without moving parts, ease of assembly and allocation, and relatively low maintenance costs [11]. Besides, in reference [12], a decentralized algorithm was proposed for energy trading among the load aggregators and renewable generators in power distribution networks, which was formulated as a bi-level optimization problem while convex relaxation techniques were used to convexify this problem.

One of the most important and typical problem of PV system operation is to extract the maximum available solar power under different atmospheric conditions, which is called maximum power point tracking (MPPT) [13] and has attracted an enormous amount of research interests. Conventional MPPT techniques own the elegant advantages of structure simplicity and fast seeking rate, such as hill-climbing [14], perturb & observe (P&O) [15], and incremental conductance (INC) [16]. Hence, they have been widely adopted and could obtain a satisfactory MPPT performance under the uniform solar irradiation scenario, e.g., all PV cells in the same module and all modules in the same string receive the identical solar irradiation and temperature, upon which there exists merely a single maximum power point (MPP).

However, partial shading condition (PSC) often occurs when there are mismatching conditions (manufacturers' tolerances of PV cell characteristics and different shading luminosity) between the solar panels of a string [17]. One feasible solution to protect the PV panels from the hot spot effect is to utilize bypass diodes connected in parallel with each PV module. More specifically, if the current of a shaded solar panel is smaller than the current of the string, then it will be shunted by the corresponding bypass diode [18]. Basically, the use of bypass diode will result in several malignant drawbacks, e.g., additional power losses, increase of overall costs, and appearance of undesirable multiple local MPPs (LMPPs). Unfortunately, the aforementioned conventional MPPT techniques cannot distinguish the difference between the LMPP and global MPP (GMPP), which will be stagnated at the first peak they encounter

regardless of whether it is a LMPP or GMPP, and are frequently trapped at a LMPP. Thus, a considerable amount of power losses will occur under PSC.

In order to remedy this thorny obstacle, plenty of power optimizers or distributed maximum power point trackers (DMPPTs) have been employed. In essence, they replace the passive bypass diodes with active devices, like power converters, such that the LMPPs can be then eliminated thus the overall power-voltage (*P-V*) characteristics could contain merely a single MPP. Such techniques can be referred to micro-inverters [19], PV voltage equalizer [20], and series/parallel connected DMPPT [21],[22]. Nevertheless, these approaches are usually very expensive which limit their applications in practice, particularly in large-scale PV stations.

On the other hand, an enormous variety of meta-heuristic based MPPT algorithms has been proposed in recent years to resolve the PSC. In literature [23], a fuzzy logic controller (FLC) was designed for MPPT, in which the near optimum design for membership functions and control rules are found simultaneously by genetic algorithm (GA). Moreover, an improved particle swarm optimization (PSO) adopting variable sampling time strategy was proposed to efficiently track the GMPP [24]. Besides, ant colony optimization (ACO) algorithm was developed with the advantages of fewer control parameters and independent convergence with the initial operation conditions [25]. Further, reference [26] applied Cuckoo search algorithm (CSA) to rapidly seek GMPP, which convergence is accelerated via Lévy flight. In addition, teaching-learning-based optimization (TLBO) was employed to exactly track the GMPP under PSC, which structure is very simple with fast convergence [27]. Besides, work [28] presented a flower pollination algorithm (FPA) to mitigate PSC in building integrated PV power systems. Meanwhile, whale optimization algorithm (WOA) was utilized for a quick and oscillation-free MPPT in the presence of PSC, which just requires few parameters and the computational burden is relatively low [29]. Based on the swarm population, literature [30] adopted radial movement optimization (RMO) associated with spherical boundaries in the search-space to handle PSC, which only needs to adjust few number of parameters to make the searching process robust and fast. In reference [31], shuffled frog leap algorithm (SFLA) was conducted to efficiently and effectively identify the GMPP under PSC. Additionally, mine blast optimization (MBO) was devised to achieve a satisfactory MPPT under different patterns of shadow [32]. Furthermore, grey wolf optimizer (GWO) was applied on PV systems under PSC, which has a fast identification speed of GMPP [33]. Besides, cat swarm optimization (CSO) was presented in work [34] to rapidly converge to GMPP in the presence of multiple peaks. In literature [35], simulate annealing (SA) was used for GMPP tracking under PSC which owns a quite simple structure. Generally speaking, the above meta-heuristic based MPPT algorithms mainly have the following two drawbacks:

- *Larger power fluctuation:* due to the random searching mechanisms, these meta-heuristic algorithms may easily converge to different optimums in different runs under the same weather condition. Hence, it will readily lead to a larger power fluctuation of PV systems;
- *Lower power output*: since the control cycle of MPPT is ultra-short, these meta-heuristic algorithms may easily converge to a low quality optimum due to the computation time limitation and the single searching mechanism. Hence, they might be easily trapped at a low quality LMPP.

In the past two decades, collective intelligence (CI) [36] has attracted enormous attentions in various fields, including biology, social sciences, engineering, computer science, etc. CI is defined as a "*Group of individuals doing things collectively that seems intelligent*" [37], which may involve consensus, social capital and formalisms such as voting systems, social media and other means of quantifying mass activity, and strongly contribute to the shift of knowledge and power from the individual to the collective. In essence, the major advantage of CI is that it can yield a better solution via a global intelligent behaviour, e.g., cooperation or competition, with a group of individuals/agents rather than a single one. For example, Google can produce an amazingly intelligent answer to a raised question based on the collective knowledge shared/analyzed by millions of people on the internet. CI has been applied in eHealth [38], nonlinear constrained optimization [39], path planning [40], personalized tourism [41], artificial ecosystem [42], etc. Motivated by this prominent feature, this paper proposes a novel dynamic leader based CI (DLCI) for searching the GMPP of a PV system under PSC, which main contributions/novelties can be summarized as follows:

- Compared with the conventional meta-heuristic algorithms [23]-[35], DLCI can simultaneously exploit multiple searching mechanisms from various types of sub-optimizer. Hence, its convergence stability can be dramatically enhanced due to the effective collaboration among different sub-optimizers, thus the power fluctuation

of PV system can be noticeably reduced;

- A dynamic leader, which represents the best sub-optimizer at the current iteration, is selected for a deeper guidance to other sub-optimizers. Therefore, the convergence of DLCI can be significantly accelerated, such that the GMPP could be obtained with a higher probability for PV system under PSC.
- Comprehensive case studies are undertaken to verify the effectiveness and superiorities of DLCI, in which the daily field data of Hong Kong in different seasons is used to evaluate the MPPT performance. Besides, a dSpace based hardware-in-the-loop (HIL) test is carried out to validate the implementation feasibility of DLCI.

The remaining of this paper is organized as follows: Section 2 aims to develop the PV systems model under PSC; In Section 3, DLCI is proposed while its application on PV systems for MPPT under PSC is provided in Section 4; In addition, case studies are undertaken in Section 5. Moreover, dSpace based HIL test results are provided in Section 6. At last, Section 7 summarizes the whole paper.

2. Modelling of PV Systems under PSC

2.1. PV cell model

A PV cell is generally a p-n semiconductor junction diode, which converts the solar irradiation into the electricity. It consists of a light generated current source, a parallel diode, and a series resistor, respectively. Generally, PV cells are grouped together to form PV modules, which are combined in both series and parallel to provide a desired power [13]. Denote the number of PV cells in series and in parallel to be N_{s} and N_{p}, respectively. The relationship between the output current and voltage can be described by [43-45]

$$I_{\mathrm{pv}} = N_{\mathrm{p}} I_{\mathrm{g}} - N_{\mathrm{p}} I_{\mathrm{s}} \left(\exp\left[\frac{q}{AKT_{\mathrm{c}}} \left(\frac{V_{\mathrm{pv}}}{N_{\mathrm{s}}} + \frac{R_{\mathrm{s}} I_{\mathrm{pv}}}{N_{\mathrm{p}}} \right) \right] - 1 \right) \tag{1}$$

where the meaning of each symbol can be found in Nomenclature.

The generated photocurrent I_{g} is determined by the solar irradiation, as follows

$$I_{\mathrm{g}} = \left(I_{\mathrm{sc}} + k_i (T_{\mathrm{c}} - T_{\mathrm{ref}}) \right) \frac{s}{1000} \tag{2}$$

Moreover, the PV cell's saturation current I_{s} changes with the temperature based on the following relationship:

$$I_{\mathrm{s}} = I_{\mathrm{RS}} \left[\frac{T_{\mathrm{c}}}{T_{\mathrm{ref}}} \right]^3 \exp\left[\frac{qE_{\mathrm{g}}}{Ak} \left(\frac{1}{T_{\mathrm{ref}}} - \frac{1}{T_{\mathrm{c}}} \right) \right] \tag{3}$$

The above equations (1)-(3) indicate that the current generated by the PV array is simultaneously relied on the solar irradiation and temperature.

2.2 PSC phenomenon

In large PV systems or microgrids, solar panels are normally connected in series in order to increase the string voltage and in parallel to increase the power. Because of the large surface that they cover, the PV modules might be exposed at different solar irradiations, which is called PSC and becomes the major reason of power losses in PV systems. In the string of PV modules, when the PV panels have different short-circuit currents, the ones with a lower current than the string current will reverse their voltage and start to absorb power from the others. Such amount of power will be dissipated as heat. If the junction temperature or reverse voltage level is not limited, a hot spot will emerge, which then leads to a permanent damage of PV panel. Such mismatching conditions usually appear due to different solar irradiations or different shadows caused by the surrounding objects. For example, trees and houses which may shade the PV module throughout the day; PV cells mismatch which normally create an internal shading type phenomena; The passage of clouds over the PV systems that results in a varying solar irradiation [45].

To avoid the aforementioned problem, bypass diodes are usually deployed to bypass the shaded PV cells. Figure 1(a) illustrates how the bypass diode limits the reverse voltage of a shaded PV cell. When all the PV cells have the same solar irradiations, bypass diodes will be switched off, as demonstrated by Fig. 1(b). In particular, the voltage on the shaded PV cell is limited according to the following equation:

$$V_{\mathrm{reverse}} = nV_{\mathrm{oc}} + V_{\mathrm{Bdiode}} \tag{4}$$

where *n* is the number of PV cells which are not shadowed from the group of bypassed cells.

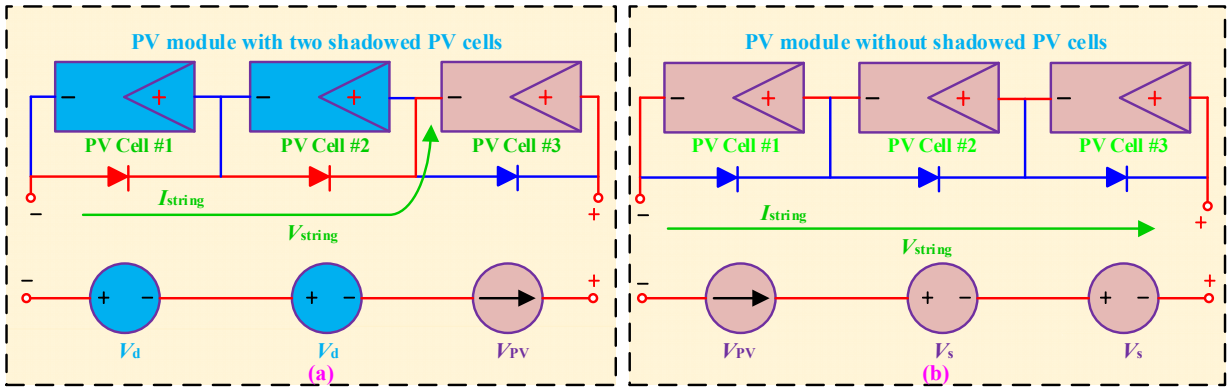

Figure 1. PV cell protection with bypass diode: (a) with shadowed PV cell; (b) without shadowed PV cell.

Generally speaking, the bypass diodes can protect the PV panels but can also decrease the harvested solar power. Moreover, the PV panels with a short-circuit current lower than the string current are shunted by the bypass diodes, by which multiple LMPPs will appear on the *P-V* characteristic, as shown in Fig. 2. Here, it is necessary that the PV system should operate at GMPP to extract the maximum available solar power from the PV array. If this is not the case, up to 70% of solar power might be lost [23].

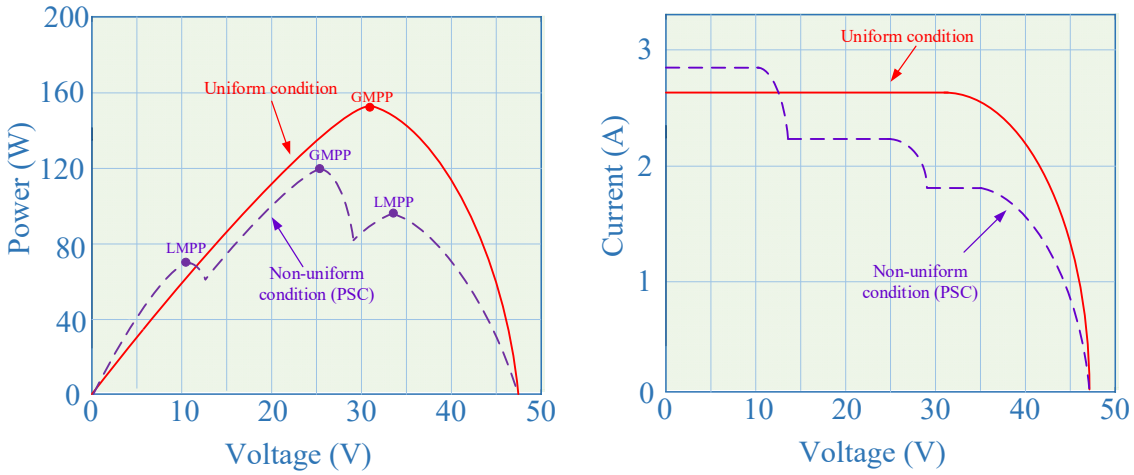

Figure 2. *P-V* curve of the PV array under PSC.

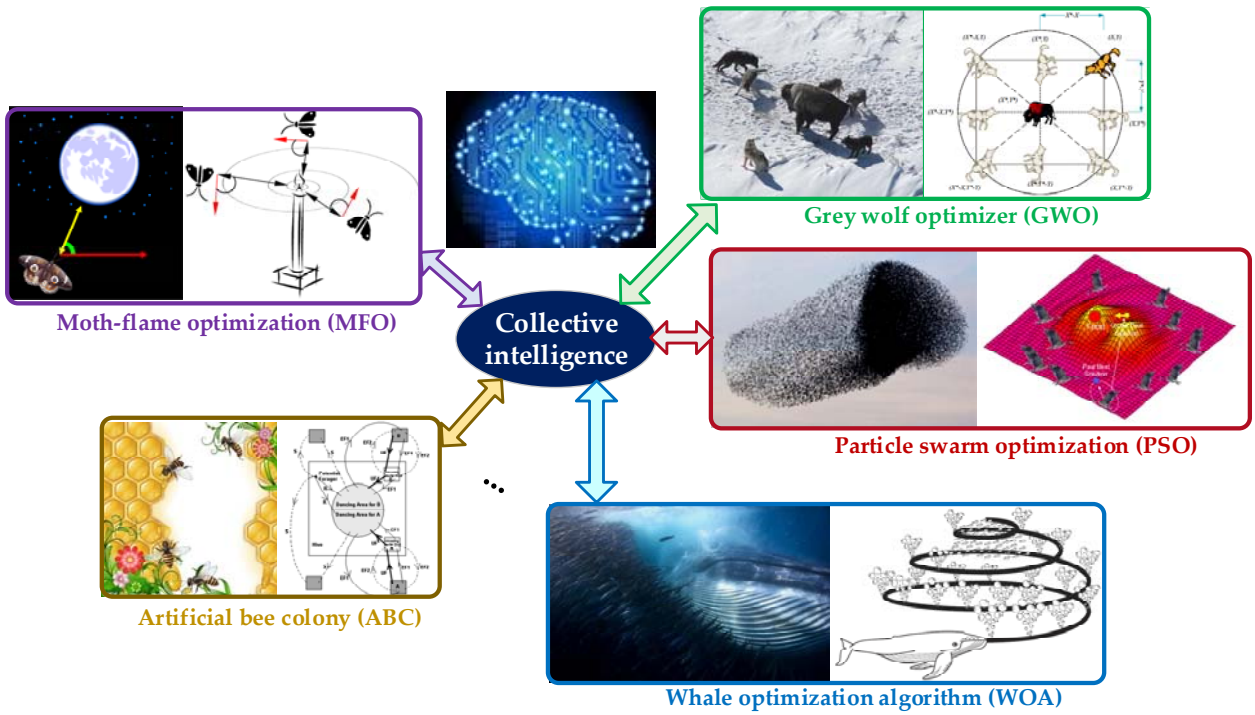

Figure 3. Optimization framework of DLCI.

3 Dynamic Leader based Collective Intelligence

As shown in Fig. 3, DLCI is consisted of various sub-optimizers. For an optimization task, each sub-optimizer can independently search an optimum, and can cooperate with the dynamic leader to improve the optimum quality.

3.1. Collective intelligence with various sub-optimizers

Each sub-optimizer can be chosen from any optimization algorithms, while the number of sub-optimizers is a user-defined parameter determined according to the requirement of a specific optimization problem. In general, a larger number of sub-optimizers will lead to a higher quality optimum due to the search diversity, but also consume more computation resources and longer computation time. In order to balance them, five methods including GWO [46], whale optimization algorithm (WOA) [47], moth-flame optimization (MFO) [48], artificial bee colony (ABC) [49], and PSO [50], are selected as the sub-optimizers of DLCI due to the following reasons [46]:

1) They are all frequently-used swarm intelligence algorithms, which is easier to be integrated into a hybrid optimization method to exploit their own advantages.

2) They not only have fewer parameters to adjust, but also have less operators compared to other evolutionary algorithms. Hence, these five sub-optimizers are easy to be implemented with a short computation time.

3) They can all utilize memory to save the current best solution obtained, which can significantly accelerate the convergence and improve the local searching ability.

The main optimization mechanism of each sub-optimizer is introduced as follows:

- *GWO*: which is inspired by the grey wolf hunting behaviour in the wild forest. In the presence of different leadership hierarchy in a grey wolf tribe, the grey wolves are divided into four roles, i.e., alpha, beta, delta, and omega, where the first three wolves are the three most dominant wolves with the smallest fitness functions. Since the hunting strategy is guided by them, all the wolves can update their positions by [46]

$$\vec{D}_\alpha = \left|\vec{C}_1 \cdot \vec{X}_\alpha - \vec{X}\right|, \vec{D}_\beta = \left|\vec{C}_2 \cdot \vec{X}_\beta - \vec{X}\right|, \vec{D}_\delta = \left|\vec{C}_3 \cdot \vec{X}_\delta - \vec{X}\right| \tag{5}$$

$$\vec{X}_1 = \vec{X}_\alpha - \vec{A}_1 \cdot \left(\vec{D}_\alpha\right), \vec{X}_2 = \vec{X}_\beta - \vec{A}_2 \cdot \left(\vec{D}_\beta\right), \vec{X}_3 = \vec{X}_\delta - \vec{A}_3 \cdot \left(\vec{D}_\delta\right) \tag{6}$$

$$\vec{X}(k+1) = \frac{\vec{X}_1 + \vec{X}_2 + \vec{X}_3}{3} \tag{7}$$

where k is the iteration index; $\vec{A}_1$, $\vec{A}_2$, $\vec{A}_3$, $\vec{C}_1$, $\vec{C}_2$, and $\vec{C}_3$ are the coefficient vectors; α, β, and δ represent the three most dominant wolves; and $\vec{X}$ denotes the position vector of a grey wolf, respectively.

- *WOA*: which is motivated by the social behaviour of humpback whales in the ocean. In order to successfully catch a prey, the humpback whale evolves the bubble-net attacking strategy to encircle the prey. During the hunting process, the humpback whales implement a shrinking circle and a spiral-shaped path simultaneously, which can be described as follows [47]:

$$\vec{D} = \left|\vec{C} \cdot \vec{X}^*(k) - \vec{X}(k)\right|, \overrightarrow{D'} = \left|\vec{X}^*(k) - \vec{X}(k)\right| \tag{8}$$

$$\vec{X}(k+1) = \begin{cases} \vec{X}^*(k) - \vec{A} \cdot \vec{D}, & \text{if } p < 0.5 \text{ (shrinking circle)} \\ \overrightarrow{D'} \cdot e^{bl} \cdot \cos(2\pi l) + \vec{X}^*(k), & \text{if } p \geq 0.5 \text{ (spiral} - \text{shaped)} \end{cases} \tag{9}$$

where $\vec{A}$ and $\vec{C}$ are the coefficient vectors; $\vec{X}^*(k)$ is the position vector of the best solution at the kth iteration; b denotes the shape constant of the logarithmic spiral; l represents a random number in [-1, 1]; and p is a random number in [0, 1], respectively.

- *MFO*: which is originated from the navigation method of moths circled around artificial lights in the night. Here, a logarithmic spiral is used for imitating the flight path of moths to the flames, in which the position vector can be updated by [48]

$$N_{\mathrm{f}}(k) = round\left(N_{\mathrm{f}}^{\max} - k * \frac{N_{\mathrm{f}}^{\max} - 1}{k_{\max}}\right) \tag{10}$$

$$\overrightarrow{D_\iota} = \left|\overrightarrow{F_J}(k) - \overrightarrow{X_\iota}(k)\right| \tag{11}$$

$$\overrightarrow{X_\iota}(k+1) = \overrightarrow{D_\iota} \cdot e^{bl} \cdot \cos(2\pi l) + \overrightarrow{F_J}(k) \tag{12}$$

where N_{f} is the number of flames; $N_{\mathrm{f}}^{\max}$ represents the maximum number of flames; $k_{\max}$ denotes the maximum iteration number; $\overrightarrow{F_J}$ is the position vector of the jth flame; and $\overrightarrow{X_\iota}$ is the position vector of the ith moth, respectively.

- *ABC*: which is derived from the foraging behaviour and waggle dance behaviour of honey bee swarm in the hive. According to different division in a hive, the honey bee swarm is classified into three groups, i.e., the employed

bees, the onlooker bees, and the scout bees. For each employed bee, the position can be updated for approximating to other solution, as follows [49]:

$$\overrightarrow{X_{\imath d}}(k+1) = \overrightarrow{X_{\imath d}}(k) + \emptyset_{id}\left(\overrightarrow{X_{\imath d}}(k) - \overrightarrow{X_{hd}}(k)\right) \tag{13}$$

where $\overrightarrow{X_{\imath d}}$ is the *d*th dimension position of the *i*th honey bee; *d* is a randomly chosen dimension; *h* denotes a randomly selected honey bee in the swarm, with $h \neq i$; and $\emptyset_{id}$ represents a random number distributed in [-1, 1], respectively.

For each onlooker bee, it will select a honey bee as a target food source from the swarm according to their fitness functions. In particular, the probability of selecting the *i*th honey bee is written as

$$p_i(k) = 0.9 \times \frac{\max_{j=1,2,..,N} f_j(k) - f_i(k)}{\max_{j=1,2,..,N} f_j(k) - \min_{j=1,2,..,N} f_j(k)} + 0.1 \tag{14}$$

where f_i is the fitness function of the *i*th honey bee, which is designed for the minimization problem; and *N* is the population size.

After determining the target food source, each onlooker bee can update its position according to (13). On the other hand, if a food source is depleted by a honey bee within a predetermined number of iterations, then the corresponding bee will be regarded as a scout bee for a random search, as follows:

$$\overrightarrow{X_\imath}(k+1) = \overrightarrow{X^{\min}} + r \cdot \left(\overrightarrow{X^{\max}} - \overrightarrow{X^{\min}}\right) \tag{15}$$

where $\overrightarrow{X^{\min}}$ and $\overrightarrow{X^{\max}}$ are the minimum and maximum position vector, respectively; and r is a random number distributed in [0,1].

- *PSO*: which is developed from the intelligent behaviour of bird flocking in the sky. At each iteration, every particle moves toward the individual best position and the global best position simultaneously, which yields [50]:

$$\vec{V}_\imath(k+1) = \omega\vec{V}_\imath(k) + c_1 r_1\left(\vec{P}_\imath(k) - \overrightarrow{X_\imath}(k)\right) + c_2 r_2\left(\vec{G}(k) - \overrightarrow{X_\imath}(k)\right) \tag{16}$$

$$\overrightarrow{X_\imath}(k+1) = \overrightarrow{X_\imath}(k) + \vec{V}_\imath(k+1) \tag{17}$$

where $\vec{V}_\imath$ is the velocity vector of the *i*th particle; ω represents the inertia weight; c_1 and c_2 are the acceleration coefficients; r_1 and r_2 are the random numbers, which range from 0 to 1; $\vec{P}_\imath$ is the individual best position of the *i*th particle; and $\vec{G}$ is the global best position of the whole swarm, respectively.

3.2. Dynamic leader based guidance

In order to accelerate the convergence of DLCI, a dynamic leader based guidance is introduced to achieve an effective coordination/collaboration between different sub-optimizers. Here, the sub-optimizer with the current best solution is chosen as the dynamic leader, as follows:

$$L = \arg\max_{o=1,2,\ldots,n} f_o^{\text{best}}(k) \tag{18}$$

where *L* represents the dynamic leader; $f_o^{\text{best}}(k)$ is the fitness function of the best solution obtained by the *o*th sub-optimizer at the *k*th iteration; and *n* is the number of sub-optimizers, respectively.

After a sub-optimizer is chosen as the dynamic leader, it will transmit the current global best solution and the corresponding fitness function to other sub-optimizers, as schematically illustrated in Fig. 4. Then, the other sub-optimizers will replace their worst solutions with the current global best solution. However, if this guidance process is implemented on each iteration, DLCI may be easily trapped into a low quality optimum. Therefore, it will be implemented on every three iterations in this paper, as follows:

$$\vec{X}_o^{\text{worst}}(k) = \begin{cases} \vec{X}_L^{\text{best}}(k), & \text{if } \frac{k}{3} \in \boldsymbol{Z} \\ \vec{X}_o^{\text{worst}}(k), & \text{otherwise} \end{cases} \tag{19}$$

where $\vec{X}_o^{\text{worst}}(k)$ is the worst solution obtained by the *o*th sub-optimizer at the *k*th iteration; $\vec{X}_L^{\text{best}}(k)$ denotes the best solution obtained by the dynamic leader at the *k*th iteration; and $\boldsymbol{Z}$ is the set of all integers, respectively.

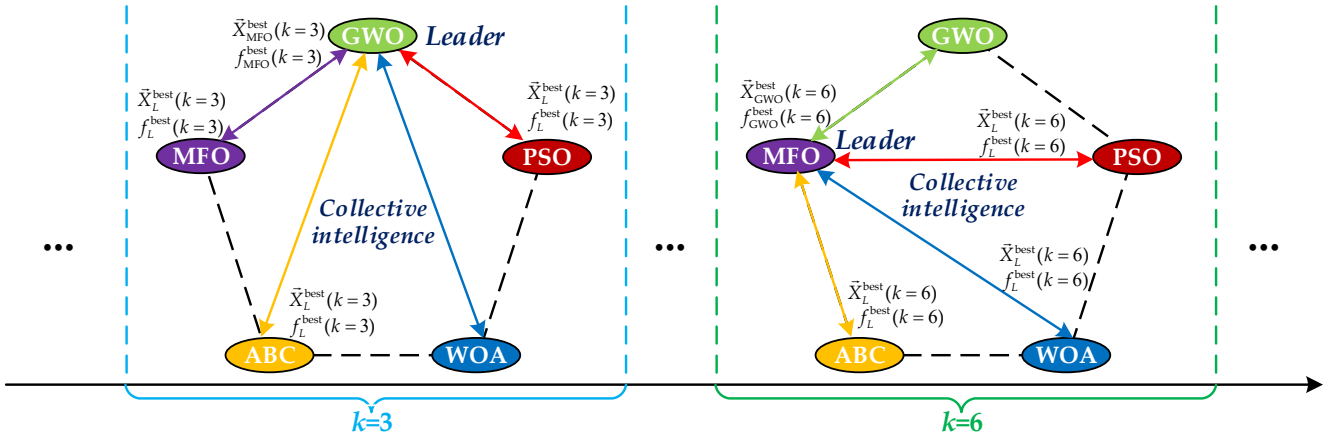

Figure 4. Dynamic leader based guidance for collective intelligence.

4 DLCI Design of PV systems for MPPT under PSC

4.1 Optimization model for MPPT under PSC

In general, the MPPT of PV systems can be achieved by regulating its output voltage V_{pv}. Since the PV system aims to maximize the active power, the optimization model for MPPT under PSC can be described as

$$\min f(V_{\mathrm{pv}}) = -P_{\mathrm{out}}(V_{\mathrm{pv}}) = -V_{\mathrm{pv}} * I_{\mathrm{pv}}(V_{\mathrm{pv}}) \tag{20}$$

$$\text{s.t. } V_{\mathrm{pv}}^{\min} \le V_{\mathrm{pv}} \le V_{\mathrm{pv}}^{\max} \tag{21}$$

where P_{out} is the active power of PV systems; $V_{\mathrm{pv}}^{\min}$ and $V_{\mathrm{pv}}^{\max}$ are the minimum and maximum output voltages of PV systems, respectively.

Note that the output current I_{pv} in (20) is mainly determined by the output voltage, temperature, solar irradiation, and PSC. For the meta-heuristic algorithms and DLCI, it searches the MPP of PV systems under PSC according to the power characteristics described by (20).

4.2 Parameters setting

Since the proposed DLCI is consisted of five swarm intelligence algorithms, plenty of algorithm parameters need to be carefully set to ensure a satisfactory optimization performance. However, it will result in a dramatic computation cost during the trial-and-error. Hence, only the two most critical parameters, i.e., the population size N and the maximum iteration number $k_{\max}$, are determined via the trial-and-error technique. In general, a larger population size and a larger maximum iteration number will obtain a higher quality optimum with a larger probability, but will also lead to a significant computation burden.

Remark 1. Note that the maximum iteration number $k_{\max}$ is regarded as the termination condition in this paper, which is more suitable to limit the computation time compared with the fitness function deviation due to the random search. Therefore, the computation time of DLCI can be guaranteed for online optimization of MPPT.

Lastly, other parameters are simply set to be the commonly used values, as tabulated in Table 1.

Table 1. The main parameters of each sub-optimizer of DLCI

Sub-optimizer	Parameters	Value
GWO	Adaption factor a	$2-\frac{2k}{k_{\max}}$
WOA	Adaption factor a	$2-\frac{2k}{k_{\max}}$
	Shape constant b	1
MFO	Maximum number of flames $N_f^{\max}$	8
	Shape constant b	1
	Linearly decreasing factor a	$-1-\frac{k}{k_{\max}}$
ABC	Number of employed bees	8
	Number of onlookers	6
	Number of scouts	3
	Limit	3
PSO	Acceleration coefficients c1/c2	2/1
	Minimum inertia	0.6
	Maximum inertia	0.85

4.3 Overall execution procedure

To this end, the overall execution procedure of DLCI based MPPT of PV systems under PSC is illustrated by Fig. 5, in which the implementation process of each sub-optimizer is executed in parallel so as to reduce the execution time. Besides, Figure 6 illustrates the overview of DLCI based MPPT of PV system under PSC.

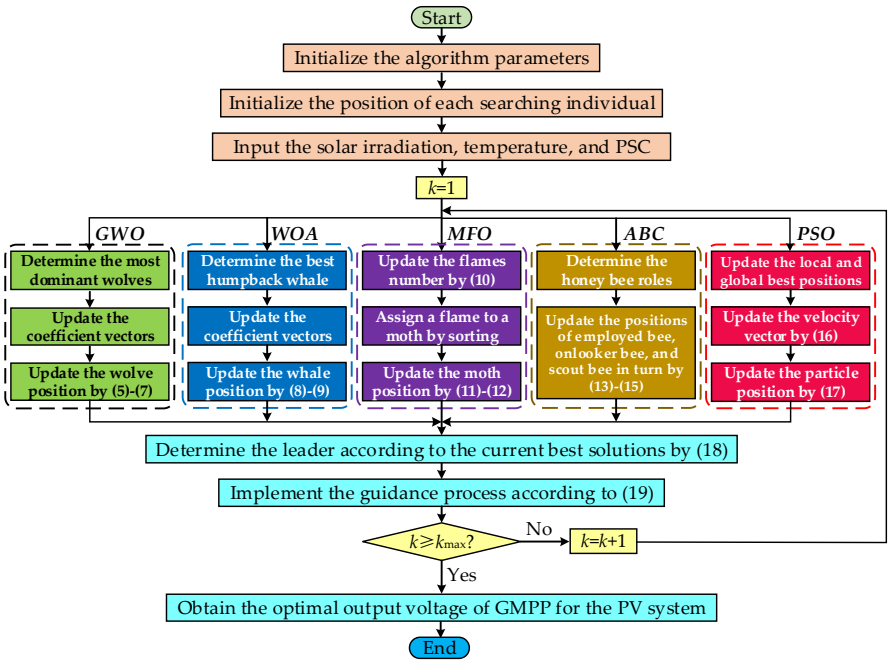

Figure 5. Overall execution procedure of DLCI for MPPT of PV systems under PSC.

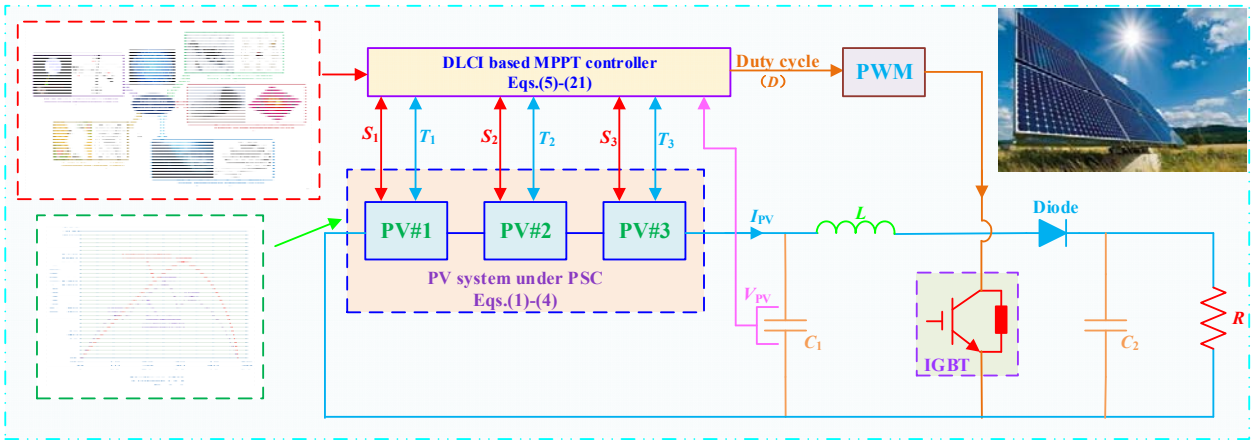

Figure 6. Schematic overview of DLCI based MPPT of PV system under PSC.

5 Case Studies

In this section, four cases, e.g., (a) Start-up test; (b) Step change in solar irradiation with constant temperature; (c) Gradual change in both solar irradiation and temperature; and (d) Daily field data of solar irradiation and temperature in Hong Kong, are carried out to evaluate the MPPT performance of DLCI under PSC, which is compared to that of INC [16], GA [23], PSO [24], ABC [25], CSA [26], GWO [33], MFO [48], WOA [47], TLBO [27], respectively. For a fair comparison among the last eight meta-heuristic algorithms, the population size and the maximum iteration number are set to be identical, e.g., N=8 and k_{max}=10, respectively. The simulation is executed on Matlab/Simulink 2016a using a personal computer with an Intel^{R} CoreTMi7 CPU at 2.2 GHz and 16 GB of RAM. The solver is ode 45 (Dormand-Prince) with an auto variable-step size.

Figure 7 shows the simulation model for MPPT under PSC developed in Matlab/Simulink environment, in which a buck-boost converter operating in the continuous inductor current mode is adopted thanks to its prominent advantages analyzed in reference [45]. In addition, Table 2 provides the PV system parameters. In order to quantitatively evaluate the power fluctuation of PV system, two indices are introduced in the case studies, which are designed as follows:

$$\Delta v^{\text{avg}} = \frac{1}{T-1}\sum_{t=2}^{T}\frac{|P_{\text{out}}(t)-P_{\text{out}}(t-1)|}{P_{\text{out}}^{\text{avg}}} \tag{22}$$

$$\Delta v^{\text{max}} = \max_{t=2,3,\ldots,T}\frac{|P_{\text{out}}(t)-P_{\text{out}}(t-1)|}{P_{\text{out}}^{\text{avg}}} \tag{23}$$

where Δv^{avg} and Δv^{max} denote the average variability and the maximum variability of power output of PV system, respectively; t is the time period; T is the total operation period; and $P_{\text{out}}^{\text{avg}}$ is the average power output of PV system over the total operation period, respectively.

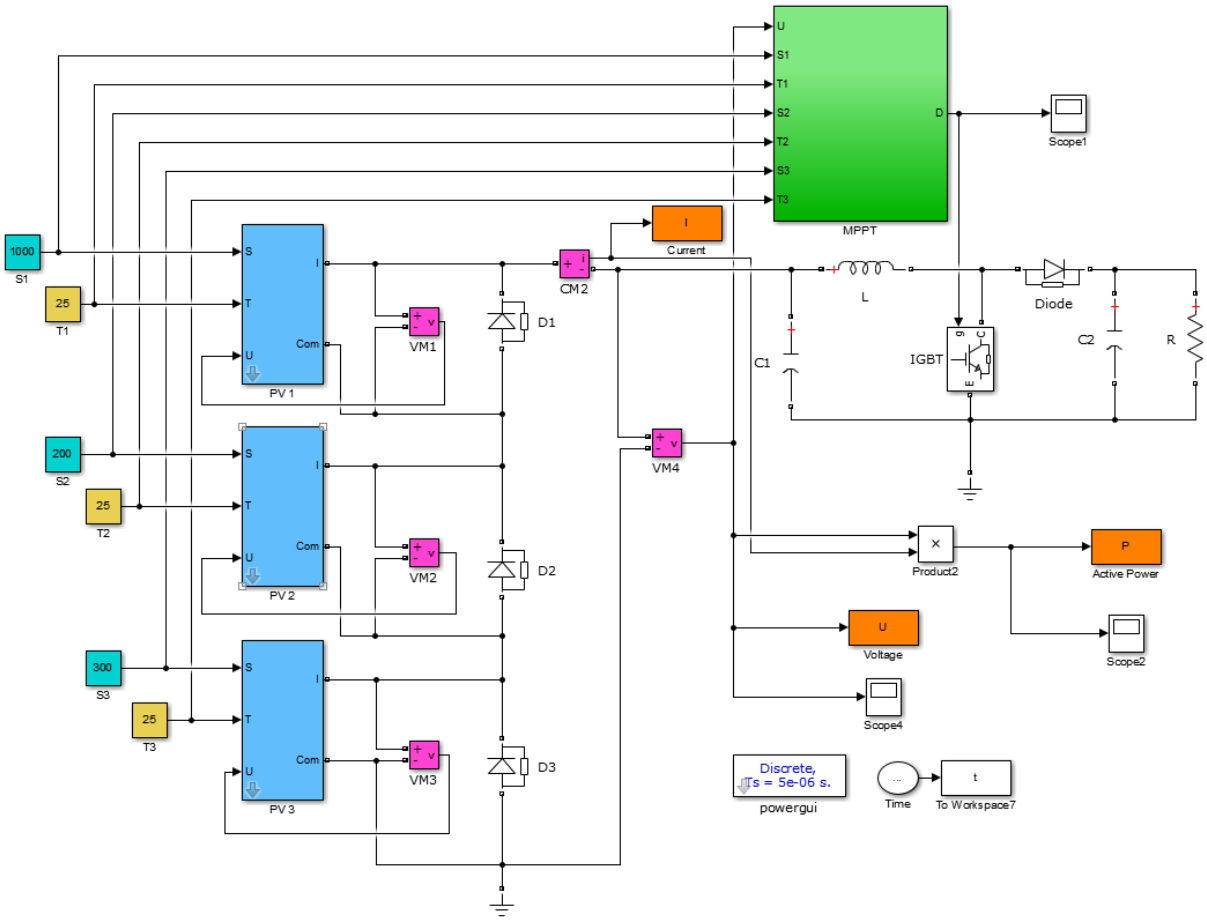

Figure 7. Simulation model for MPPT under PSC using Matlab/Simulink.

Moreover, the rated solar irradiation and temperature are set as 1000 W/m^2 and 25℃, respectively. Under such standard conditions, the PV power P_{out}=51.716 W, PV output voltage V_{pv}=18.47 V, and PV output current I_{pv}=2.8 A, respectively.

Table 2. The PV system parameters

Typical peak power	51.716W	**Nominal operation cell temperature (T_{ref})**	25℃
Voltage at peak power	18.47V	**p-n junction ideality factor (A)**	1.5
Current at peak power	2.8A	**Switching frequency (f)**	100 kHz
Short-circuit current (I_{sc})	1.5A	**Inductor (L)**	500 mH
Open-circuit voltage (V_{oc})	23.36V	**Resistive load (R)**	200 Ω
Temperature coefficient of I_{sc} (k_1)	3mA/℃	**Capacitor(C_1,C_2)**	1 μF

5.1 Start-up test

This test attempts to evaluate the MPPT speed and convergence stability at start-up (from zero point). In order to simulate the effect of PSC, the solar irradiation of three PV arrays are chosen to be 1000 W/m^2, 200 W/m^2, and 300 W/m^2, respectively. Here, Figure 8 demonstrates the online optimization results of different algorithms for MPPT. One can readily observe that INC is able to converge to a stable point with a much shorter period of time than that of others. However, it is inevitably trapped at a low quality LMPP as it cannot distinguish the difference between GMPP and LMPP. Besides, it also presents a consistent oscillation at the steady state, which is much more significant than that of other meta-heuristic algorithms. In contrast, other meta-heuristic algorithms can effectively escape from the LMPP thanks to their elegant global searching mechanism. As given in Table 3, the DLCI based MPPT can generate the highest energy, together with the lowest power fluctuations. More specifically, the obtained energy by DLCI can

generate 35.64% than that of INC, while the obtained average variability of PSO is about 5 times of that obtained by DLCI. As a consequence, the results of Fig. 8 and Table 3 demonstrate that the CI associated with various sub-optimizers can greatly improve the global searching ability and convergence stability, while the dynamic leader based guidance can noticeably enhance the local searching ability.

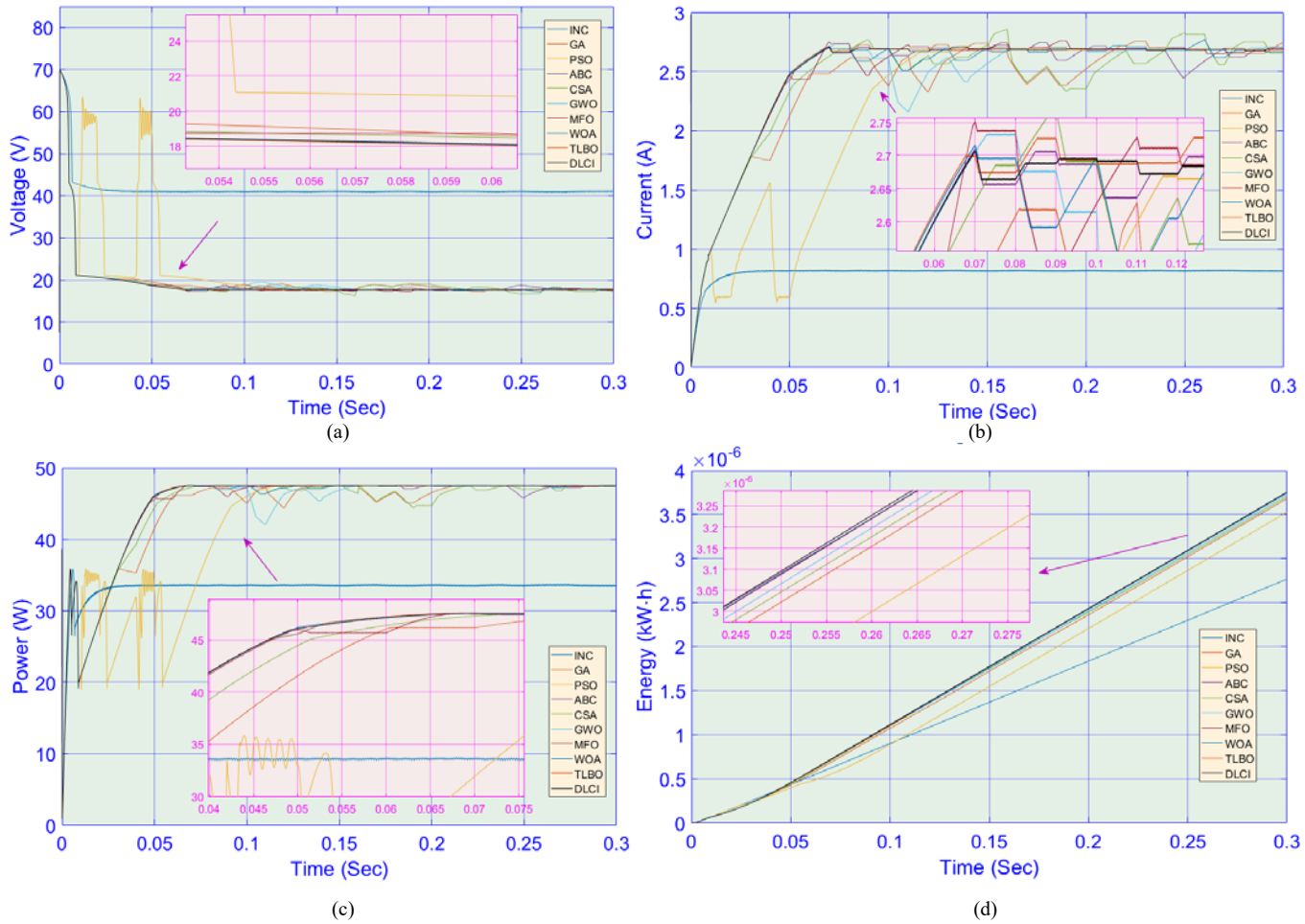

Figure 8. PV system responses of ten methods obtained under the start-up test. (a) Voltage, (b) Current, (c) Power, and (d) Energy.

Table 3. Statistical results obtained by ten methods under the start-up test.

Indices	INC	GA	PSO	ABC	CSA	GWO	MFO	WOA	TLBO	DLCI
Energy (10^{-6} kW·h)	2.7687	3.6814	3.5273	3.7477	3.7033	3.7255	3.7469	3.7482	3.7554	**3.7555**
Δv^{max}	0.0518%	0.0326%	2.5039%	0.0249%	0.0590%	0.0441%	0.0254%	0.0221%	0.0126%	**0.0109%**
Δv^{avg}	0.0218%	0.0039%	0.0099%	0.0024%	0.0039%	0.0030%	0.0023%	0.0025%	0.0020%	**0.0020%**

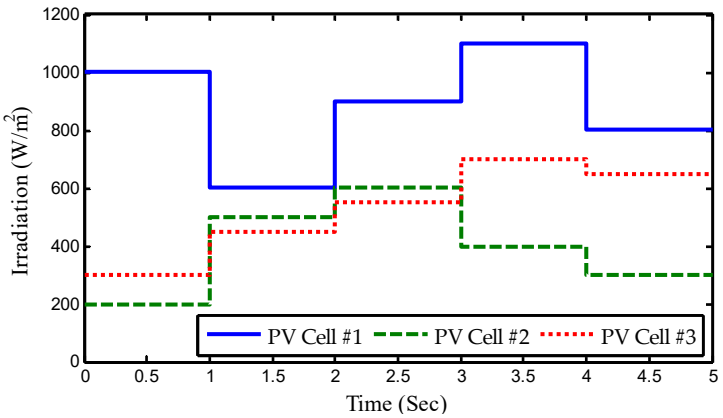

Figure 9. Step change of solar irradiation with PSC.

5.2 Step change in solar irradiation with constant temperature

The step change in solar irradiation is usually emerged when a cloud rapidly passes over a PV array. In order to evaluate the MPPT performance of DLCI under such case, four consecutive solar irradiation steps are applied on the PV array, as clearly depicted by Fig. 9, of which the step change occurs at every second interval. During the test, the temperature is maintained at the rated value, e.g., 25℃.

Figure 10 provides the online optimization results of different algorithms for MPPT in the presence of step change in solar irradiation. Similar to the start-up test, the PV system can generate much more energy by the meta-heuristic algorithms compared to that of INC under the same weather conditions. Particularly, DLCI can produce the largest energy, which is capable of generating an additional 24.54 % energy than that of INC, as shown in Table 4. On the other hand, it produces just the smallest power fluctuation (Δv^{max} and Δv^{avg}) when the solar irradiation suddenly changes at each interval, while other meta-heuristic algorithms are however prone to such transient process. This verifies that the incorporation of various sub-optimizers associated with different searching mechanisms can effectively guarantee the convergence stability of DLCI.

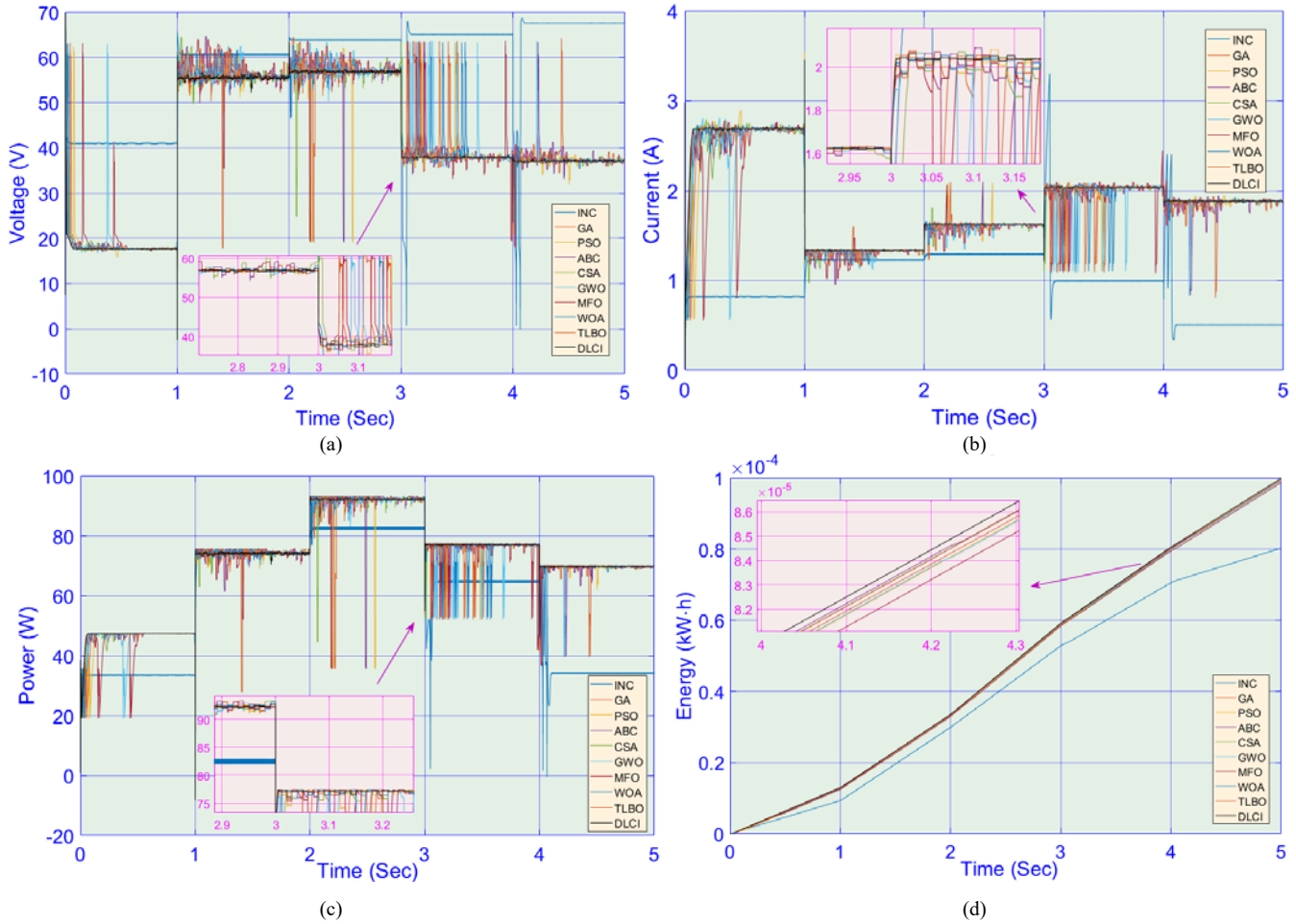

Figure 10. PV system responses of ten methods obtained under the step change in solar irradiation with constant temperature. (a) Voltage, (b) Current, (c) Power, and (d) Energy.

Table 4. Statistical results obtained by ten methods under the step change test.

Indices	INC	GA	PSO	ABC	CSA	GWO	MFO	WOA	TLBO	DLCI
Energy (10^{-6} kW·h)	80.2585	99.2695	99.1924	99.5503	99.5812	99.1720	98.7283	99.5658	99.5738	**99.9561**
Δv^{max}	43.5967%	34.3194%	34.3122%	34.1791%	32.0816%	34.3135%	34.5096%	33.4909%	34.1927%	**34.0296%**
Δv^{avg}	0.0324%	0.0078%	0.0080%	0.0075%	0.0076%	0.0079%	0.0087%	0.0074%	0.0075%	**0.0069%**

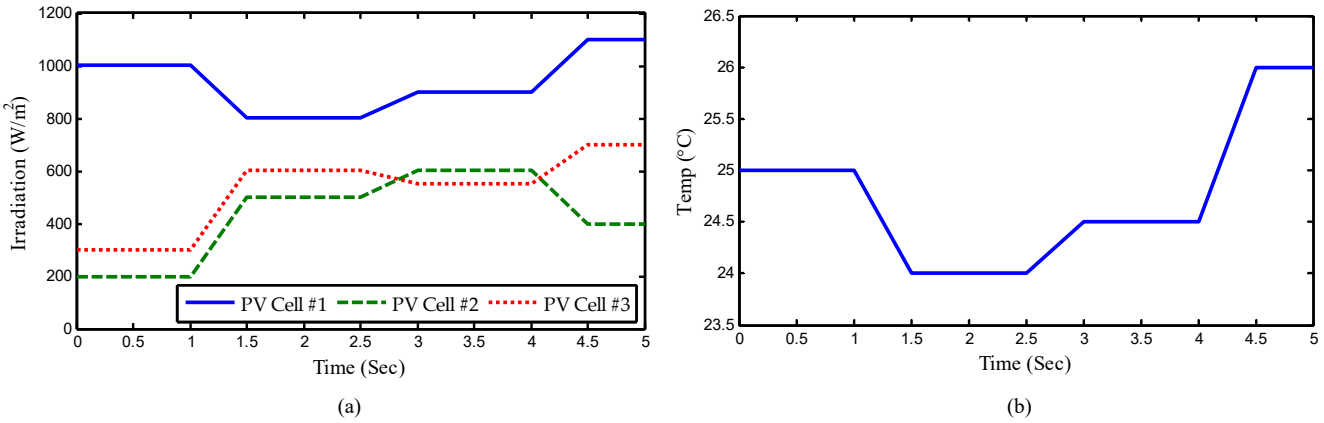

(a) (b)

Figure 11. Gradual change in both solar irradiation and temperature. (a) Solar irradiation and (b) Temperature.

5.3 Gradual change in both solar irradiation and temperature

In a typical sunny day, both the solar irradiation and temperature will increase as the hour approaches midday and thereafter decreases towards the evening. In order to investigate the MPPT performance of DLIC under such gradual changes, e.g., a ramp change in both solar irradiation and temperature is emulated over a time period of 5 *s*, as depicted in Fig. 11.

Both Figure 12 and Table 5 provide the results of ten algorithms for MPPT obtained under gradual change in both solar irradiation and temperature. One can find that the meta-heuristic algorithms except DLCI still result in larger power fluctuations even under the relatively slow gradual change in both solar irradiation and temperature. In contrast, by employing various sub-optimizers for MPPT, DLCI can considerably reduce the power fluctuations of the PV system with a wider global searching and a deeper local searching ability. Besides, DLCI can generate the largest energy among all the algorithms, which is in excess of 11.42% to that of INC (See Table 5).

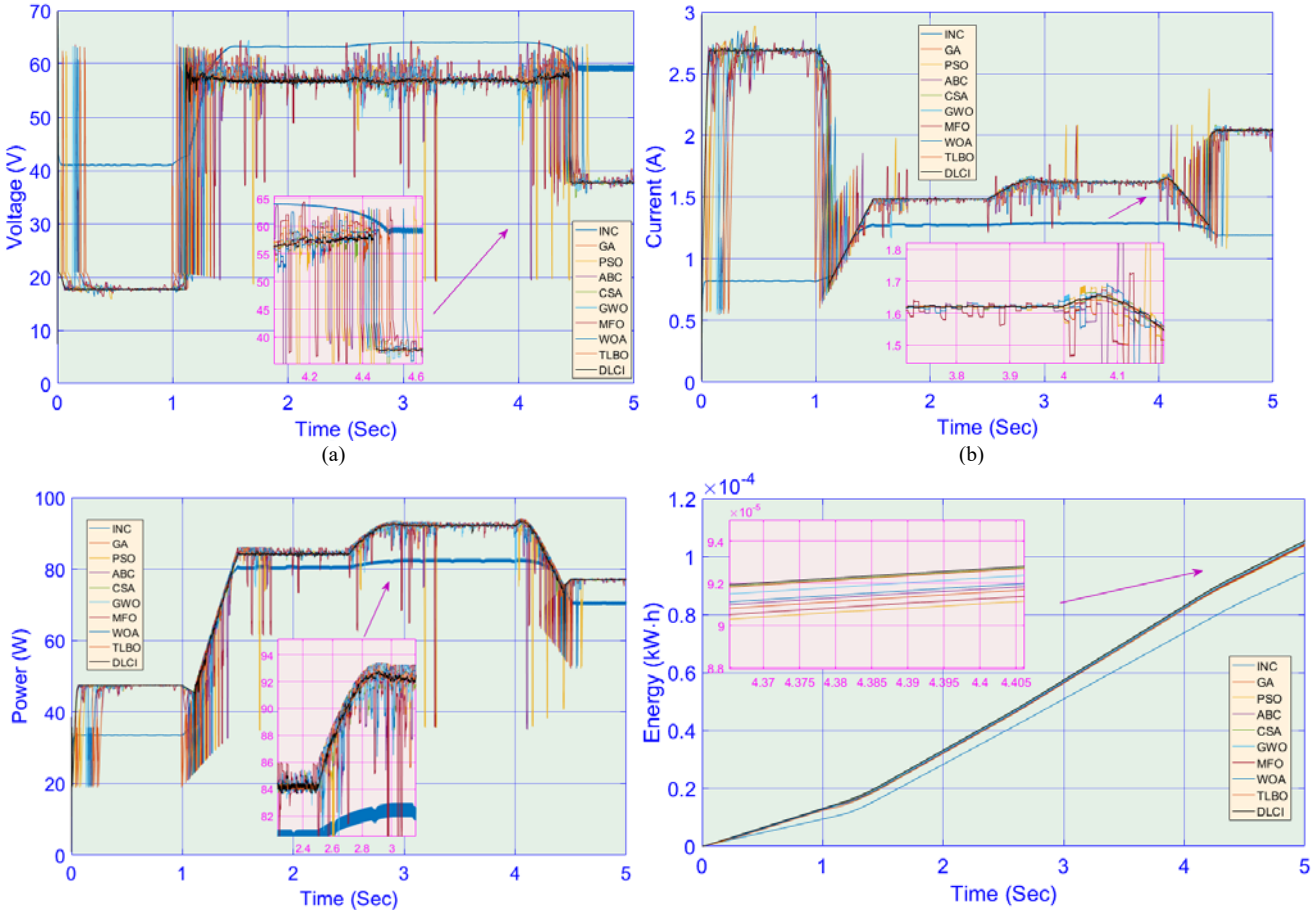

(a) (b) (c) (d)

Figure 12. PV system responses of ten methods obtained under the gradual change in both solar irradiation and temperature. (a) Voltage, (b) Current, (c) Power, and (d) Energy.

Table 5. Statistical results obtained by ten methods under the gradual change test.

Indices	INC	GA	PSO	ABC	CSA	GWO	MFO	WOA	TLBO	DLCI
Energy (10^{-6} kW·h)	94.5701	105.3233	103.6949	104.4872	105.3747	105.0092	103.9950	104.5620	104.2711	**105.4400**
Δv^{max}	24.1141%	21.6521%	21.9921%	21.8254%	21.6416%	21.7169%	21.9287%	21.8098%	21.8706%	**21.6282%**
Δv^{avg}	0.0300%	0.0074%	0.0099%	0.0092%	0.0073%	0.0079%	0.0097%	0.0084%	0.0085%	**0.0070%**

5.4 Daily field data of solar irradiation and temperature in Hong Kong

To further evaluate the MPPT performance of DLCI, the PV system is simulated for MPPT with the actual measured field data of solar irradiation and temperature in Hong Kong, which locates at the subtropical region on the eastern side of the Pearl River estuary in south China. (See Fig. 13). In Hong Kong, summer is hot and humid with occasional showers and thunderstorms. Typhoons most often occur in summer, sometimes resulting in flooding or landslides. Winters are mild and usually start sunny, becoming cloudier towards February; the occasional cold front brings strong, cooling winds from the north. The most temperate seasons are spring, which can be changeable, and autumn, which is generally sunny and dry [51]. The measured data is chosen from four typical days of four seasons in 2013, where the data interval is 10 *min*. The detailed geographical position of the measurement device is shown in Fig. 14, which coordinates are at 22.3 degree north latitude and at 114.2 degree east longitude. To imitate PSC, the solar irradiations of PV cells #1 to #3 are set to be 100%, 80%, and 50% of the actual solar irradiation, respectively.

Figure 15 and Figure 16 provide the obtained power and energy of eight algorithms for MPPT under different typical days in four seasons. It can be seen that all the meta-heuristic algorithms can generate higher energy than that of INC at most of the time. Furthermore, DLCI can make the PV system generate the largest energy in different seasons, which is up to 116.43% to that of INC in the winter, as illustrated in Table 6. From the whole simulation period, the power fluctuations obtained by DLCI are still much smaller than other algorithms in spring and summer.

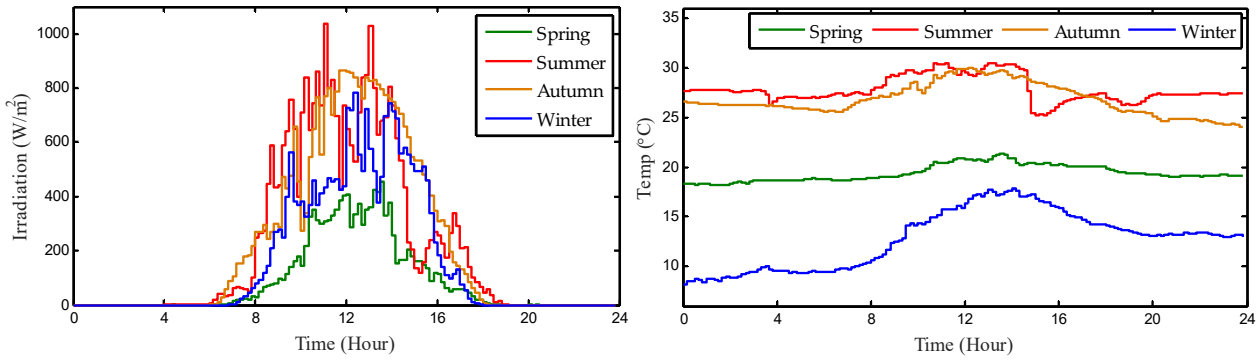

(a) (b)

Figure 13. Daily field profile of solar irradiation and temperature in Hong Kong. (a) Irradiation and (b) Temperature.

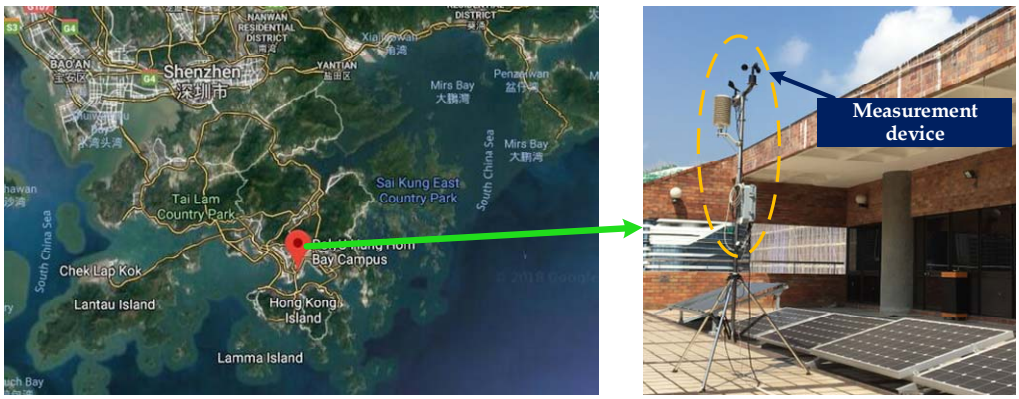

Figure 14. The detailed geographical position of the measurement device for solar irradiation and temperature.

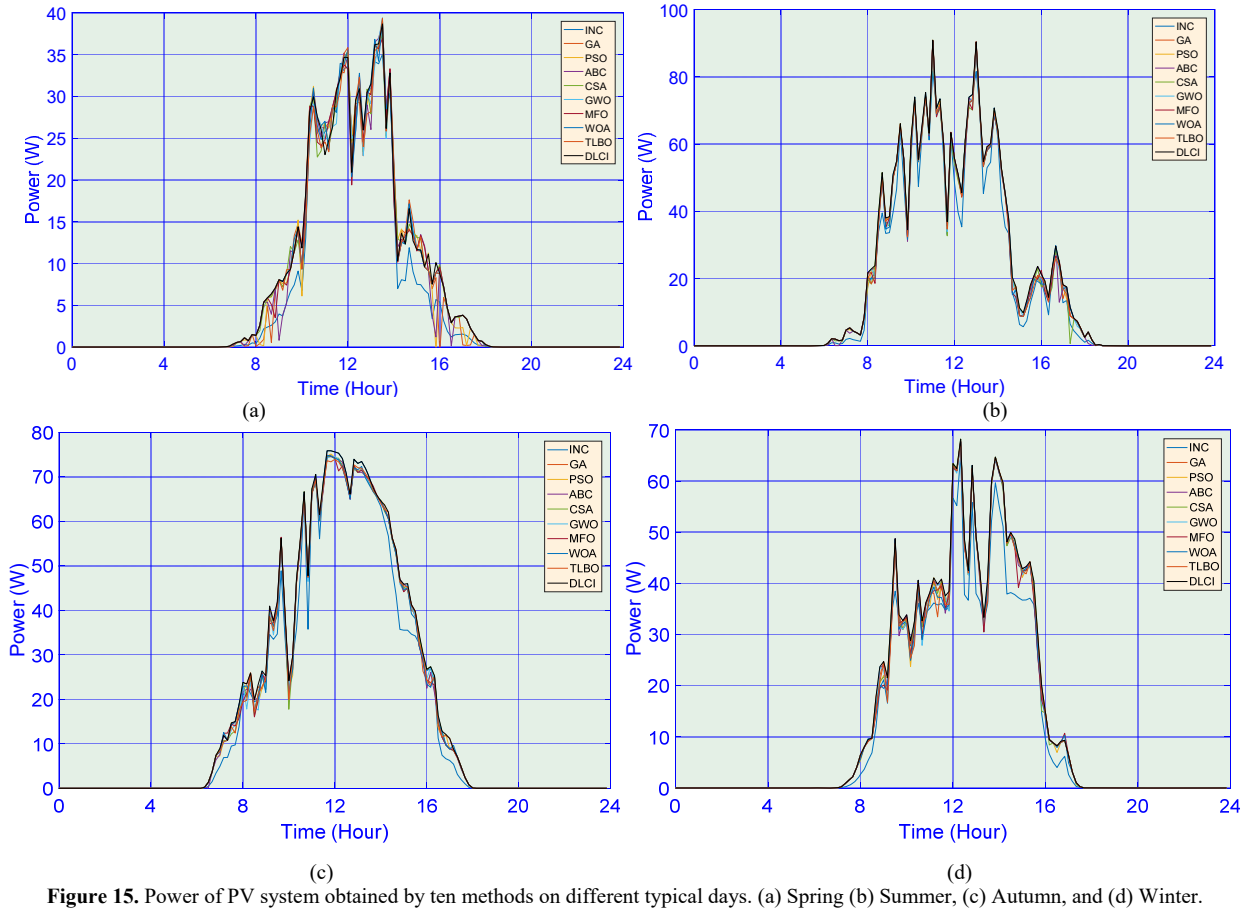

Figure 15. Power of PV system obtained by ten methods on different typical days. (a) Spring (b) Summer, (c) Autumn, and (d) Winter.

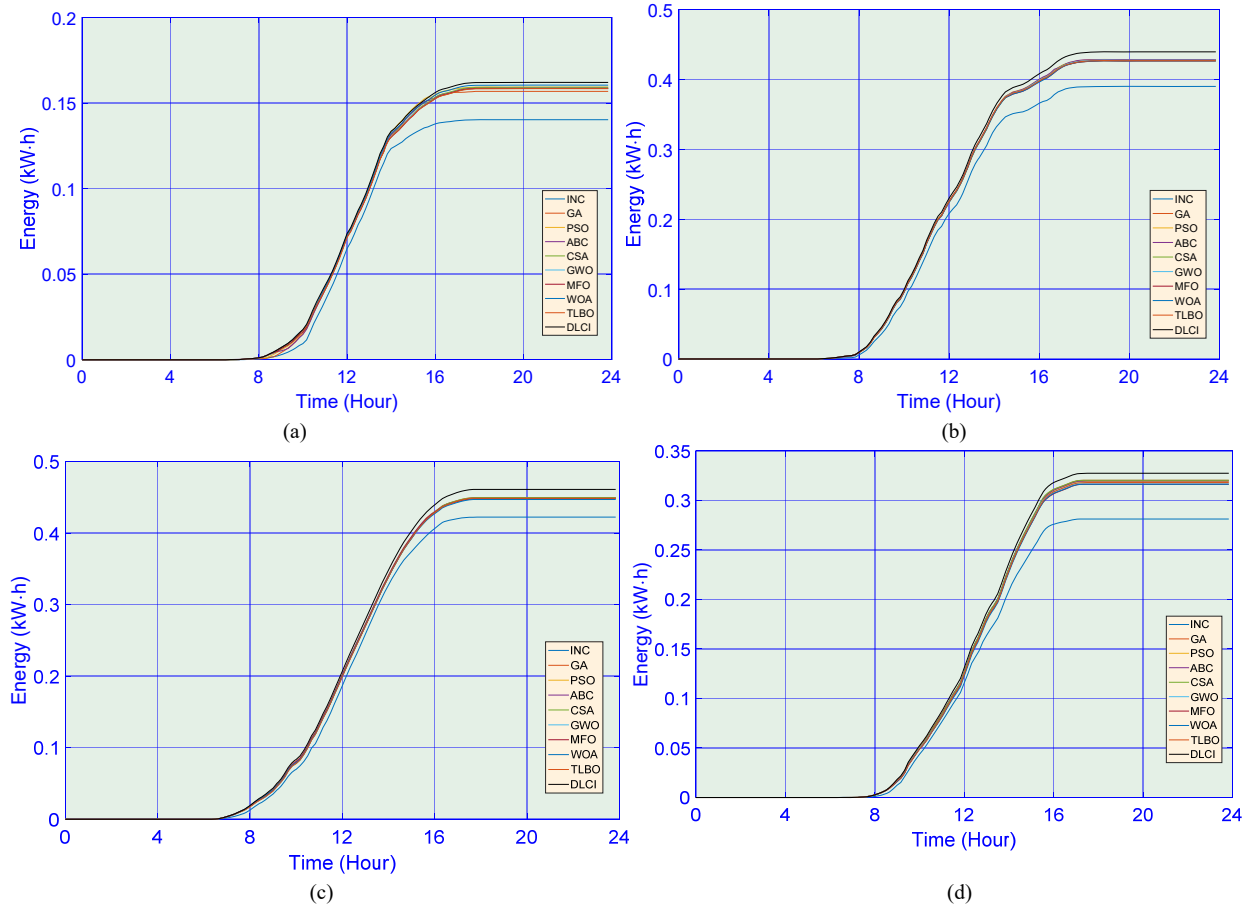

Figure 16. Energy of PV system obtained by ten methods on different typical days. (a) Spring (b) Summer, (c) Autumn, and (d) Winter.

Table 6. Statistical results obtained by ten methods under the practical test in Hong Kong.

Season	Indices	INC	GA	PSO	ABC	CSA	GWO	MFO	WOA	TLBO	DLCI
Spring	Energy (kW·h)	0.1403	0.1569	0.1593	0.1586	0.1592	0.1587	0.1587	0.1605	0.1584	**0.1621**
	$\Delta v^{\max}$	257.46%	183.48%	178.24%	163.03%	212.33%	226.58%	239.02%	227.40%	216.22%	**203.35%**
	Δv^{avg}	17.96%	19.31%	20.30%	21.24%	18.32%	18.14%	18.08%	18.82%	18.79%	**17.95%**
Summer	Energy (kW·h)	0.3902	0.4282	0.4288	0.4285	0.4268	0.4279	0.4267	0.4270	0.4272	**0.4397**
	$\Delta v^{\max}$	174.36%	166.10%	158.78%	166.02%	157.23%	164.72%	158.37%	163.87%	160.78%	**151.16%**
	Δv^{avg}	25.93%	22.79%	22.40%	23.23%	23.30%	22.47%	23.33%	22.82%	22.84%	**22.18%**
Autumn	Energy (kW·h)	0.4222	0.4495	0.4486	0.4490	0.4495	0.4477	0.4480	0.4470	0.4487	**0.4610**
	$\Delta v^{\max}$	173.21%	106.35%	113.15%	105.17%	112.72%	107.30%	98.18%	105.98%	105.04%	**101.78%**
	Δv^{avg}	13.34%	11.46%	11.83%	**11.38%**	12.28%	12.64%	11.71%	11.96%	11.77%	11.41%
Winter	Energy (kW·h)	0.2812	0.3203	0.3192	0.3196	0.3204	0.3176	0.3163	0.3163	0.3180	**0.3274**
	$\Delta v^{\max}$	234.77%	212.16%	188.74%	183.83%	198.02%	212.85%	187.79%	206.13%	204.26%	**182.94%**
	Δv^{avg}	**16.46%**	17.61%	18.37%	18.07%	17.30%	18.62%	17.94%	17.50%	18.04%	16.61%

5.5 Performance comparisons of DLCI with different numbers of sub-optimizers

Generally speaking, DLCI associated with larger number of sub-optimizers will obtain a higher quality optimum for MPPT, but it also consumes more computation time. In order to investigate this feature, DLCI with four, five, and six sub-optimizers are executed for performance comparisons, where the original DLCI excluding the sub-optimizer of PSO is taken as the DLCI with four sub-optimizers; and the original DLCI with an additional sub-optimizer of CSA is taken as the DLCI with six sub-optimizers. Table 7 provides the statistical results obtained by the above three DLCIs under different cases. Firstly, it is obvious that the computation time of DLCI grows as the number of sub-optimizers increases. However, they can all satisfy the online optimization for MPPT of PV system. Secondly, DLCI associated with larger number of sub-optimizers can make the PV system generate more energy, which verifies that a larger number of sub-optimizers can improve the searching ability. Thirdly, the power fluctuation ($\Delta v^{\max}$ and Δv^{avg}) of PV system can be reduced by using a larger number of sub-optimizers. Although DLCI with six sub-optimizers outperforms that with five sub-optimizers, their performance are very close. Hence, This paper chooses five sub-optimizers based DLCI to achieve a more proper trade-off between the computation time and the optimum quality.

Table 7. Statistical results obtained by DLCI with different numbers of sub-optimizers under different tests.

Scenario		Indices	Number of sub-optimizers		
			4	5	6
Start-up		Computation time (Sec)	0.0038	0.0043	0.0052
		Energy (10^{-6} kW·h)	3.7538	3.7555	3.7555
		$\Delta v^{\max}$	0.0175%	0.0109%	0.0109%
		Δv^{avg}	0.0021%	0.0020%	0.0020%
Step change		Computation time (Sec)	0.0038	0.0042	0.0050
		Energy (10^{-6} kW·h)	99.9458	99.9561	99.9570
		$\Delta v^{\max}$	34.0668%	34.0296%	33.0288%
		Δv^{avg}	0.0069%	0.0069%	0.0069%
Gradual change		Computation time (Sec)	0.0042	0.0046	0.0053
		Energy (10^{-6} kW·h)	105.4247	105.4400	105.4406
		$\Delta v^{\max}$	21.6313%	21.6282%	21.6257%
		Δv^{avg}	0.0071%	0.0070%	0.0070%
Hong Kong	Spring	Computation time (Sec)	0.0038	0.0041	0.0053
		Energy (kW·h)	0.1599	0.1621	0.1622
		$\Delta v^{\max}$	204.22%	203.35%	202.10%
		Δv^{avg}	18.08%	17.95%	17.91%
	Summer	Computation time (Sec)	0.004	0.0046	0.0054
		Energy (kW·h)	0.4296	0.4397	0.4398
		$\Delta v^{\max}$	155.89%	151.16%	151.13%
		Δv^{avg}	22.76%	22.18%	22.17%
	Autumn	Computation time (Sec)	0.0041	0.0046	0.0055
		Energy (kW·h)	0.4575	0.4610	0.4611
		$\Delta v^{\max}$	103.34%	101.78%	101.66%
		Δv^{avg}	11.65%	11.41%	11.40%
	Winter	Computation time (Sec)	0.0039	0.0045	0.0053
		Energy (kW·h)	0.3188	0.3274	0.3274
		$\Delta v^{\max}$	184.47%	182.94%	182.90%
		Δv^{avg}	17.21%	16.61%	16.61%

6. HIL Test

HIL test can provide an important and reliable tool to evaluate and justify the complex/complicated real-time embedded systems via applying the complexity of the controlled system to the test platform [5]. It has validated the implementation feasibility of different MPPT strategies of PV systems [44, 52, 53].

A dSpace based HIL test is carried out, which configuration and experiment platform are illustrated in Fig. 17 and Fig. 18, respectively. More specifically, DLCI based MPPT algorithm (5)-(19) is embedded on one dSpace platform (DS1104 board) with a sampling frequency f_c=10 kHz. Meanwhile, the PV system (1)-(4), solar irradiation and temperature simulator is implemented on another dSpace platform (DS1006 board) with a limit sampling frequency f_s=100 kHz to emulate the PSC effect and various atmospheric conditions. Here the solar irradiation and temperature are measured from the real-time simulation of the PV system (1)-(4) on the DS1006 board, which are then transmitted online to DLCI based MPPT algorithm (5)-(19) embedded on the DS1104 board for the real-time calculation of output voltage V_{pv}.

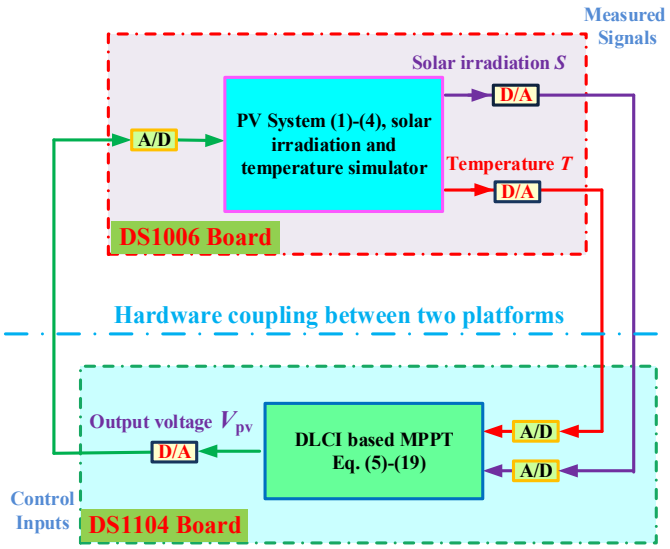

Figure 17. The configuration of HIL test.

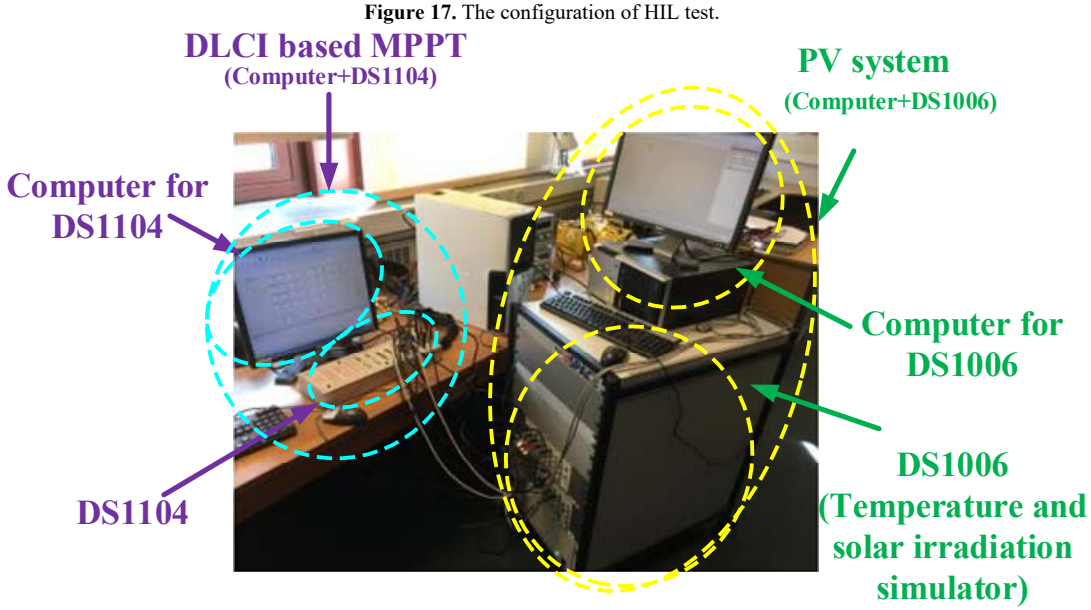

Figure 18. The hardware platform of HIL test.

6.1 HIL results of start-up test

Figure 19 demonstrates the comparison of simulation results and HIL test results obtained by start-up test. It is clear to find that their results are very similar, which validates the implementation feasibility of DLIC based MPPT.

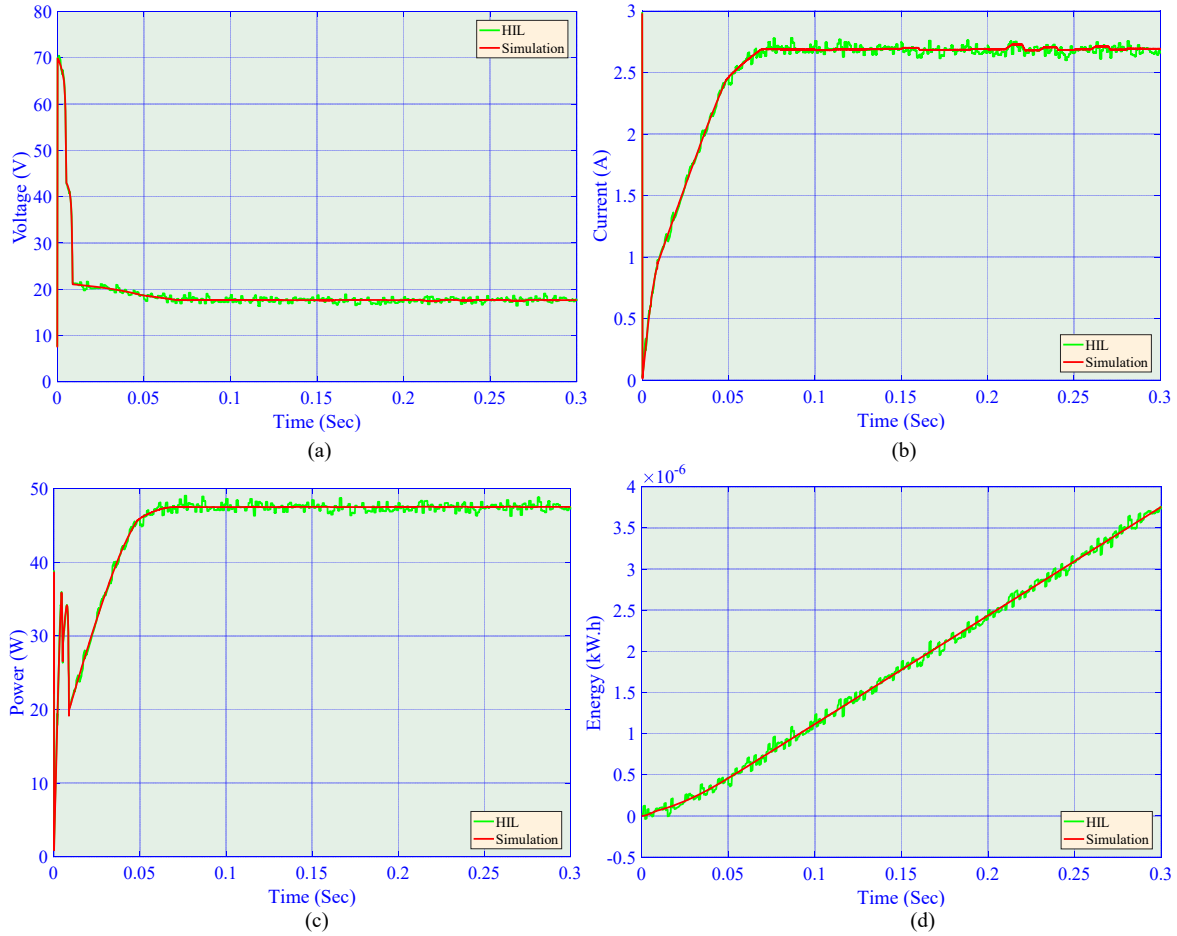

Figure 19. The simulation results and HIL test results obtained under the start-up test. (a) Voltage, (b) Current, (c) Power, and (d) Energy.

6.2 HIL results of step change in solar irradiation with constant temperature

The simulation results and HIL test results obtained by step change in solar irradiation with constant temperature is compared in Figure 20. One can readily observe that their responses are very close despite of some oscillations appeared in HIL test.

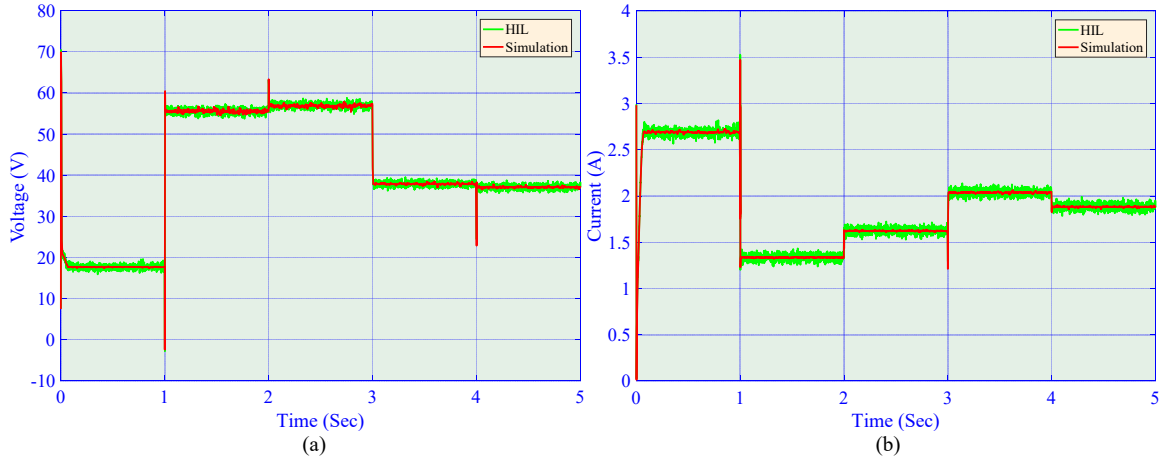

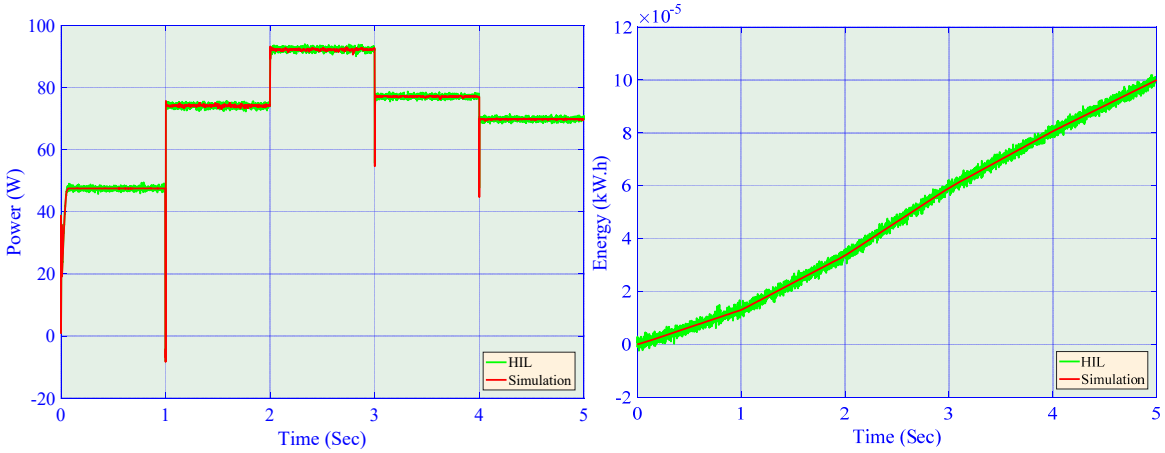

Figure 20. The simulation results and HIL test results obtained under the step change in solar irradiation with constant temperature. (a) Voltage, (b) Current, (c) Power, and (d) Energy.

6.3 HIL results of gradual change in both solar irradiation and temperature

In Figure 21, the MPPT performance of simulation and HIL test in the presence of gradual change in both solar irradiation and temperature is illustrated. Again, they have quite similar responses and performance.

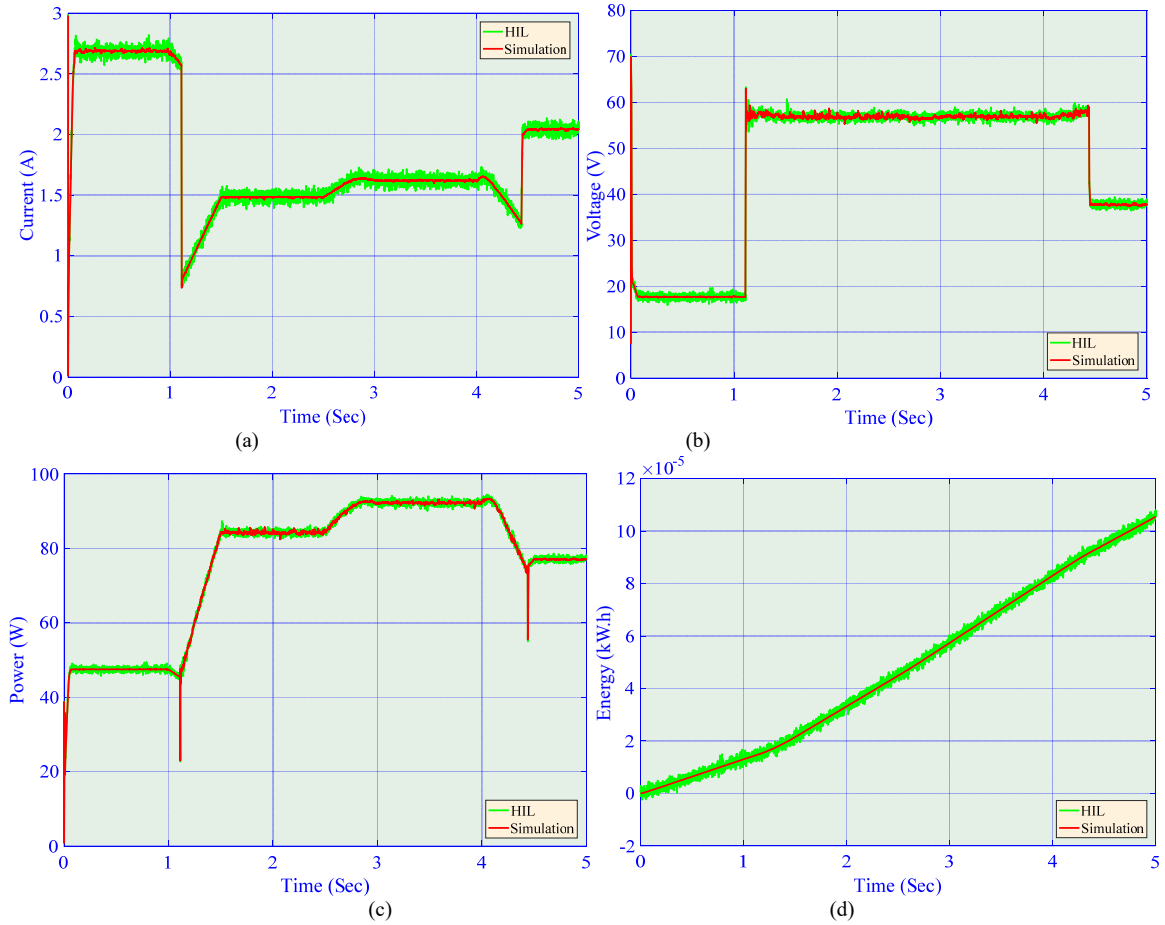

Figure 21. The simulation results and HIL test results obtained under the gradual change in both solar irradiation and temperature. (a) Voltage, (b) Current, (c) Power, and (d) Energy.

At last, the difference between the simulation results and HIL test results is mainly due to the following four reasons:

• *Measurement disturbances*: which might produce consistent oscillations in the HIL test. A filter could be adopted to greatly suppress such disturbances to improve the MPPT performance;

• *Discretization of HIL test and sampling holding*: which may bring in an additional amount of errors compared to that of the continuous control used in the simulation;

• *Time delay*: which generally results in a degradation of MPPT performance;

• *Unknown harmonics*: which is usually caused by the capacitors or inductors distributed between the signal transmission cables and the dSpace device.

7. Conclusions

This paper aims to harvest the available maximum solar energy of PV systems and rapidly achieve GMPPT in the presence of PSC. Here, a novel DLCI is designed, which incorporates various types of sub-optimizer into the CI, such that the GMPPT performance can be achieved. The contributions/main findings of this paper can be summarized as follows:

• The existing meta-heuristic algorithms based MPPT are designed with a single searching mechanism, which easily lead to a weak searching ability. In contrast, DLCI can apply multiple searching mechanisms of various sub-optimizers to MPPT, such that a deeper local searching and wider global searching can be achieved. Therefore, DLCI based MPPT can make the PV system generate more energy under PSC.

• Due to the random searching mechanism, the existing meta-heuristic algorithm may converge to different optimal solutions for MPPT in different runs under the same weather condition. In contrast, DLCI can significantly reduce the convergence randomness via the dynamic leader based guidance. Hence, it can produce much smaller power fluctuations of PV systems under PSC.

• Comprehensive case studies are undertaken to verify the effectiveness and advantages of DLCI, in which nine typical algorithms are thoroughly compared with DLCI. Moreover, a dSpace based HIL test is carried out which shows that the HIL results are very similar to that of simulation results. Simulation results demonstrate that DLCI can generate an additional amount of energy from 0.38% (against CSA) to 24.54 % (against INC) under step change in solar irradiation; 0.06% (against CSA) to 11.42 % (against INC) under gradual change in both solar irradiation and temperature; as well as 2.52% (against PSO and CSA) to 9.90% (against INC) under daily field data of solar irradiation and temperature in Hong Kong. Furthermore, DLCI can reduce the power fluctuations of PV system from 0% to 80% (against PSO under start-up test) compared with that of other eight meta-heuristic algorithms.

Future studies will implement DLIC into a microcontroller on a small-capacity PV system, in which the PV inverter part will also be considered to test its MPPT performance under a complete PV system in practice.

Acknowledgments

The authors gratefully acknowledge the support of National Natural Science Foundation of China (51477055, 51667010, 51777078).

References

[1] Yang, B.; Zhang, X.S.; Yu, T.; Shu, H.C.; Fang, Z.H. Grouped grey wolf optimizer for maximum power point tracking of doubly-fed induction generator based wind turbine. *Energy Conversion and Management* **2017**, 133: 427-443.

[2] Yang, B.; Jiang, L.; Wang, L.; Yao, W.; Wu, Q.H. Nonlinear maximum power point tracking control and modal analysis of DFIG based wind turbine. *International Journal of Electrical Power & Energy Systems* **2016**, 74: 429-436.

[3] Yang, B.; Yu, T.; Shu, H.C.; Zhang, X.S.; Qu, K.P.; Jiang, L. Democratic joint operations algorithm for optimal power extraction of PMSG based wind energy conversion system. *Energy Conversion and Management* **2018**, 159: 312-326.

[4] Yang, B.; Yu, T.; Shu, H.C.; Dong, J.; Jiang, L. Robust sliding-mode control of wind energy conversion systems for optimal power extraction via nonlinear perturbation observers, *Applied Energy* **2018**, 210: 711-723.

[5] Yang, B.; Yu, T.; Shu, H.C.; Zhang, Y.M.; Chen, J.; Sang, Y.Y.; Jiang, L. Passivity-based sliding-mode control design for optimal power extraction of a PMSG based variable speed wind turbine. *Renewable Energy* **2018**, 119: 577-589.

[6] Shen, Y.; Yao, W.; Wen, J.Y.; He, H.B. Adaptive wide-area power oscillation damper design for photovoltaic plant considering delay compensation. *IET Generation, Transmission and Distribution* **2017**, 11(18): 4511-4519.

[7] Liao, S.W.; Yao, W.; Han, X.N.; Wen, J.Y.; Cheng, S.J. Chronological operation simulation framework for regional power system under high penetration of renewable energy using meteorological data. *Applied Energy* **2017**, 203: 816-828.

[8] Liu, J.; Wen, J.Y.; Yao, W.; Long, Y. Solution to short-term frequency response of wind farms by using energy storage systems. *IET Renewable Power Generation* **2016**, 10(5): 669-678.

[9] Yao, W.; Jiang, L.; Wen, J.Y.; Wu, Q.H.; Cheng, S.J. Wide-area damping controller for power system inter-area oscillations: a networked predictive control approach. *IEEE Transactions on Control Systems Technology* **2015**, 23(1): 27-36.

[10] Shen, Y.; Yao, W.; Wen, J.Y.; He, H.B.; Chen, W.B. Adaptive supplementary damping control of VSC-HVDC for interarea oscillation using GrHDP. *IEEE Transactions on Power Systems* **2018**, 33(2): 1777-1789.

[11] Yang, B.; Yu, T.; Shu, H.C.; Zhu, D.N.; An, N.; Sang, Y.Y.; Jiang, L. Energy reshaping based passive fractional-order PID control design and implementation of a grid-connected PV inverter for MPPT using grouped grey wolf optimizer. *Solar Energy* **2018**, 170: 31-46.

[12] Bahrami, S.; Amini, M.H.; Shafie-khah, M.; Catalao, J.P.S. A decentralized renewable generation management and demand response in power distribution networks. *IEEE Transactions on Sustainable Energy* **2018**, doi: 10.1109/TSTE.2018.2815502.

[13] Kandemir, E.; Cetin, N.S.; Borekci, S. A comprehensive overview of maximum power extraction methods for PV systems. *Renewable and Sustainable Energy Reviews* **2017**, 78: 93-112.

[14] Tanaka, T.; Toumiya, T.; Suzuki, T. Output control by hill-climbing method for a small scale wind power generating system. *Renewable Energy* **2014**, 12(4): 387-400.

[15] Mohanty, S.; Subudhi, B.; Ray, P.K. A grey wolf-assisted Perturb & Observe MPPT algorithm for a PV system. *IEEE Transactions on Energy Conversion* **2017**, 32(1): 340-347.

[16] Zakzouk, N.E.; Elsaharty, M.A.; Abdelsalam, A.K; Helal, A.A. Improved performance low-cost incremental conductance PV MPPT technique. *IET Renewable Power Generation* **2016**, 10(4): 561-574.

[17] Rezk, H.; Fathy, A.; Abdelaziz, A.Y. A comparison of different global MPPT techniques based on meta-heuristic algorithms for photovoltaic system subjected to partial shading conditions. *Renewable and Sustainable Energy Reviews* **2017**, 74: 377-386.

[18] Ko, S.W.; Ju, Y.C.; Hwang, H.M.; et al. Electric and thermal characteristics of photovoltaic modules under partial shading and with a damaged bypass diode. *Energy* **2017**, 128: 232-243.

[19] Alajmi, B.N.; Ahmed, K.H.; Adam, G.P.; Williams, B.W. Single-phase single-stage transformer less grid-connected PV system. *IEEE Transactions on Industrial Electronics* **2013**, 60(6): 2664-2676.

[20] Villa, L.F.L.; Ho, T.P.; Crebier, J.C.; Raison, B. A power electronics equalizer application for partially shaded photovoltaic modules. *IEEE Transactions on Industrial Electronics* **2013**, 60(2):1179-1190.

[21] Kim, H.; Kim, J.H.; Min, B.D.; Yoo, D.W.; Kim, H.J. A highly efficient PV system using a series connection of DC-DC converter output with a photovoltaic panel. *Renewable Energy* **2009**, 34: 2432-2436.

[22] Tseng, K.C.; Huang, C.C.; Shih, W.Y. A high step-up converter with a voltage multiplier module for a photovoltaic system. *IEEE Transactions on Power Electronics* **2013**, 28(6): 3047-3557.

[23] Daraban, S.; Petreus, D.; Morel, C. A novel MPPT (maximum power point tracking) algorithm based on a modified genetic algorithm specialized on tracking the global maximum power point in photovoltaic systems affected by partial shading. *Energy* **2014**, 74(5): 374-388.

[24] Sen, T.; Pragallapati, N.; Agarwal, V.; Kumar, R. Global maximum power point tracking of PV arrays under partial shading conditions using a modified particle velocity-based PSO technique. *IET Renewable Power Generation* **2018**, 12(5): 555-564.

[25] Titri, S.; Larbes, C.; Toumi, K.; Benatchba, K. A new MPPT controller based on the ant colony optimization algorithm for photovoltaic systems under partial shading conditions. *Applied Soft Computing* **2017**, 58: 465-479.

[26] Ahmed, J.; Salam, Z. A maximum power point tracking (MPPT) for PV system using Cuckoo search with partial shading capability. *Applied Energy* **2014**, 119: 118-130.

[27] Rezk, H.; Fathy, A. Simulation of global MPPT based on teaching-learning-based optimization technique for partially shaded PV system. *Electrical Engineering* **2017**, 99: 847-859.

[28] Diab, A.A.Z.; Rezk, H. Global MPPT based on flower pollination and differential evolution algorithms to mitigate partial shading in building integrated PV system. *Solar Energy* **2017**, 157: 171-186.

[29] Kumar, N.; Hussain, I.; Singh, B.; Panigrahi, B.K. MPPT in dynamic condition of partially shaded PV system by using WODE technique. *IEEE Transactions on Sustainable Energy* **2017**, 8(3): 1204-1214.

[30] Rahmani, R.; Yusof, R. A new simple, fast and efficient algorithm for global optimization over continuous search-space problems: Radial Movement Optimization. *Applied Mathematics and Computation* **2014**, 248: 287-300.

[31] Sridhar, R.; Jeevananthan, S.; Dash, S.S.; Vishnuram, P. A new maximum power tracking in PV system during partially shaded conditions based on shuffled frog leap algorithm. *Journal of Experimental and Theoretical Artificial Intelligence* **2016**, 29(3): 481-493.

[32] Fathy, A.; Rezk, H. A novel methodology for simulating maximum power point trackers using mine blast optimization and teaching learning based optimization algorithms for partially shaded photovoltaic system. *Journal of Renewable and Sustainable Energy* **2016**, 8(2): 718-726.

[33] Mohanty, S.; Subudhi, B.; Ray, P. K. A new MPPT design using grey wolf optimization technique for photovoltaic system under partial shading conditions. *IEEE Transactions on Sustainable Energy* **2015**, 7(1): 181-188.

[34] Guo, L.; Meng, Z.; Sun, Y.; Wang, L. A modified cat swarm optimization based maximum power point tracking method for photovoltaic system under partially shaded condition. *Energy* **2018**, 144, 501-514.

[35] Lyden, S.; Haque, M.E. A simulated annealing global maximum power point tracking approach for PV modules under partial shading conditions. *IEEE Transactions on Power Electronics* **2016**, 31(6): 4171-4181.

[36] Levy, P; Bononno R. Collective intelligence: mankind's emerging world in cyberspace. Cambridge, Mass: Basic Books, 1999.

[37] Schut, M. C. Scientific handbook of simulation of collective intelligence **2007**, https://www.cs.vu.nl/~schut/dbldot/collectivae/sci/sci.pdf

[38] Camacho A.; Merayo. M. G.; Núñez, M. Collective intelligence and databases in eHealth: A survey1. *Journal of Intelligent & Fuzzy Systems* **2016**, 32(2):1-12.

[39] De-Los-Cobos-Silva, S. G.; Mora-Gutiérrez, R. A.; Gutiérrez-Andrade, M. A.; et al. Development of seven hybrid methods based on collective intelligence for solving nonlinear constrained optimization problems. *Artificial Intelligence Review* **2016**: 1-35.

[40] Jha, D. K.; Chattopadhyay, P.; Sarkar, S.; et al. Path planning in GPS-denied environments via collective intelligence of distributed sensor networks. *International Journal of Control* **2016**, 89(5): 1-24.

[41] Shen, J.; Deng, C.; Gao, X. Attraction recommendation: Towards personalized tourism via collective intelligence. *Neurocomputing* **2016**, 173: 789-798.

[42] Asgari, A.; Hassani, K.; Lee, W. S. Simulating collective intelligence of bio-inspired competing agents. *Expert Systems with Applications* **2016**, 56: 256-267.

[43] Lalili, D.; Mellit, A.; Lourci, N.; Medjahed, B.; Boubakir, C. State feedback control and variable step size MPPT algorithm of three-level grid-connected photovoltaic inverter. *Solar Energy* **2013**, 98: 561-571.

[44] Yang, B.; Yu, T.; Shu, H.C.; Zhu, D.N.; Zeng, F.; Sang, Y.Y.; Jiang, L. Perturbation observer based fractional-order PID control of photovoltaics inverters for solar energy harvesting via Yin-Yang-Pair optimization. *Energy Conversion and Management* **2018**, 171: 170-187.

[45] Qi, J.; Zhang, Y.; Chen, Y. Modeling and maximum power point tracking (MPPT) method for PV array under partial shade conditions. *Renewable Energy* **2014**, 66: 337-345.

[46] Mirjalili, S.; Mirjalili, S. M.; Lewis, A. Grey wolf optimizer. *Advances in Engineering Software* **2014**, 69: 46-61.

[47] Mirjalili, S.; Lewis, A. The whale optimization algorithm. *Advances in Engineering Software* **2016**, 95: 51-67.

[48] Mirjalili, S. Moth-flame optimization algorithm: a novel nature-inspired heuristic paradigm. *Knowledge-Based Systems* **2015**, 89: 228-249.

[49] Xiang, W. L.; Li, Y. Z.; Meng, X. L.; Zhang, C. M.; An, M. Q. A grey artificial bee colony algorithm. *Applied Soft Computing* **2017**, 60: 1-17.

[50] Chen, Y.; Li, L.; Xiao, J.; Yang, Y.; Liang, J.; Li, T. Particle swarm optimizer with crossover operation. *Engineering Applications of Artificial Intelligence* **2018**, 70: 159-169.

[51] Chen, C. C.; Lin, B. C.; Yap, L.; Chiang, P. H.; Chan, T. C. The association between ambient temperature and acute diarrhea incidence in Hong Kong, Taiwan, and Japan. *Sustainability* **2018**, 10, 1417; doi:10.3390/su10051417.

[52] Li, X.; Wen, H.; Hu, Y.; Jiang, L.; Xiao, W. Modified beta algorithm for GMPPT and partial shading detection in photovoltaic systems. *IEEE Transactions on Power Electronics* **2018**, 33(3): 2172-2186.

[53] Yang, B.; Yu, T.; Shu, H.C.; Zhu, D.N.; An, N.; Sang, Y.Y.; Jiang, L. Perturbation observer based fractional-order sliding-mode controller for MPPT of grid-connected PV inverters: design and real-time implementation. *Control Engineering Practice* **2018**, 79: 105-125.